Titanium Stable Isotopic Variations in Chondrites, Achondrites and Lunar Rocks

Nicolas D. Greber[1,+,*], Nicolas Dauphas[1], Igor S. Puchtel[2], Beda A. Hofmann[3], Nicholas T. Arndt[4]

[1]*Origins Laboratory, Department of the Geophysical Sciences and Enrico Fermi Institute, The University of Chicago, 5734 South Ellis Avenue, Chicago, IL 60615, USA*
[2]*Department of Geology, University of Maryland, College Park, MD 20742, USA*
[3]*Naturhistorisches Museum der Burgergemeinde Bern, Bernastrasse 15, Bern, Switzerland*
[4]*Université Grenoble Alpes, Institute Science de la Terre (ISTerre), CNRS, F-38041 Grenoble, France*

Abstract

Titanium isotopes are potential tracers of processes of evaporation/condensation in the solar nebula and magmatic differentiation in planetary bodies. To gain new insights into the processes that control Ti isotopic variations in planetary materials, 25 komatiites, 15 chondrites, 11 HED-clan meteorites, 5 angrites, 6 aubrites, a martian shergottite, and a KREEP-rich impact melt breccia have been analyzed for their mass-dependent Ti isotopic compositions, presented using the δ^{49}Ti notation (deviation in permil of the ^{49}Ti/^{47}Ti ratio relative to the OL-Ti standard). No significant variation in δ^{49}Ti is found among ordinary, enstatite, and carbonaceous chondrites, and the average chondritic δ^{49}Ti value of +0.004 ± 0.010 ‰ is in excellent agreement with the published estimate for the bulk silicate Earth, the Moon, Mars, and the HED and angrite parent-bodies. The average δ^{49}Ti value of komatiites of -0.001 ± 0.019 ‰ is also identical to that of the bulk silicate Earth and chondrites. OL-Ti has a Ti isotopic composition that is indistinguishable from chondrites and is therefore a suitable material for reporting δ^{49}Ti values. Previously published isotope data on another highly refractory element, Ca, show measurable variations among chondrites. The decoupling between Ca and Ti isotope systematics most likely occurred during condensation in the solar nebula.

Aubrites exhibit significant variations in δ^{49}Ti, from -0.07 to +0.24 ‰. This is likely due to the uniquely reducing conditions under which the aubrite parent-body differentiated, allowing chalcophile Ti^{3+} and lithophile Ti^{4+} to co-exist. Consequently, the observed negative correlation between δ^{49}Ti values and MgO concentrations among aubrites is interpreted to be the result of isotope fractionation driven by the different oxidation states of Ti in this environment, such that isotopically heavy Ti^{4+} was concentrated in the residual liquid during magmatic differentiation.

Finally, KREEPy impact melt breccia Sau 169 exhibits a heavy δ^{49}Ti of +0.330 ± 0.034 ‰ which is interpreted to result from Ti isotopic fractionation during ilmenite precipitation in the late stages of lunar magma ocean crystallization. A Rayleigh distillation calculation assuming a crystallization temperature of 1175°C predicts that a δ^{49}Ti value of +0.330 ‰ is achieved after removal of 94% of the Ti in ilmenite with an ilmenite-melt Ti isotopic fractionation of -0.12‰.

1 Introduction

In recent years, a growing number of non-traditional stable isotope systems have been used to study the evolution of the Earth and other solar system bodies (Teng et al., 2017). With advances in analytical techniques, non-traditional stable isotopes have seen increasing application to investigate high-temperature processes, such as magmatic differentiation, core formation, and early solar nebula evaporation and condensation. Titanium is a refractory and fluid immobile element, whose isotopic variations have seldom been measured.

The existence of mass-dependent Ti isotope fractionation in Ca-Al-rich inclusions (CAIs) had been detected by Niederer et al. (1985), who reported a shift towards heavier Ti isotopic compositions of CAIs compared to their host meteorite. More recent studies investigating CAIs of the Allende meteorite reported variations in the δ^{49}Ti value (part per mil deviation of the ^{49}Ti/^{47}Ti ratio in a sample from that of the OL-Ti standard) ranging from -4.0 to +4.0‰ (Zhang 2012; Davis et al., 2016). This is most likely the result of kinetically driven isotope fractionation during condensation and evaporation processes.

Terrestrial rocks exhibit somewhat smaller variations in their Ti isotopic composition, with δ^{49}Ti values ranging between -0.07 and +0.55 ‰ (Millet et al., 2014; Millet et al., 2016). These variations are still significant, however, as the measurement precision achieved on δ^{49}Ti is better than ±0.03‰ (Millet et al., 2014). Titanium isotopes show little variation in mafic and ultramafic igneous rocks. Millet et al. (2016) used such rocks to estimate the Ti isotopic composition of the bulk Earth relative to the OL-Ti standard to be +0.005 ± 0.005 ‰ (95% c.i., n=30). More evolved crustal rocks are enriched in heavy Ti isotopes and δ^{49}Ti correlates well with the SiO_2 concentration (Millet et al., 2016). This systematic shift towards heavier isotope compositions has been interpreted to result from preferential incorporation of light Ti in Fe-Ti oxides during fractional crystallization, leaving behind a melt that is enriched in heavy Ti isotopes.

Previous work has revealed variations in the stable isotopic composition of Ca among bulk chondrites, demonstrating that refractory elements can be fractionated isotopically by nebular processes. Documenting whether such variations also exist for Ti is important to assess whether the bulk silicate Earth has the same isotopic composition as chondrites, and evaluate possible genetic relationships between the Earth and meteorites.

Titanium isotopes can also be used to constrain the igneous history of differentiated planetesimals. For example, Millet et al. (2016) reported small variations in the Ti isotopic composition of low-Ti and high-Ti lunar mare basalts, whereby the latter have a heavier δ^{49}Ti value. It is generally thought that ilmenite cumulates in the lunar mantle are involved in the production of high-Ti lunar mare basalts. Taking Ti isotope variation in evolved terrestrial silicic rocks as a guide, ilmenite is expected to have a light Ti isotopic composition relative to the melt. To explain the heavy δ^{49}Ti value in high-Ti mare basalts, Millet et al. (2016) argued that they were likely sourced from mantle regions fertilized by negatively buoyant partial melts of ilmenite cumulates or that ilmenite was not exhausted during the melting process. In both cases, high-Ti lunar mare basalt melt would have become enriched in heavy Ti isotopes by equilibrating with isotopically light ilmenite. The model proposed by Millet et al., (2016) for the Ti isotope evolution during the lunar magma ocean predicts that the residual liquid after ilmenite crystallization would be strongly enriched in heavy Ti isotopes. Accordingly, KREEP-rich lunar samples, rocks highly enriched in incompatible trace elements and thought to represent leftover melt after major ilmenite crystallization in the lunar magma ocean (e.g., Warren and Wasson 1979), are expected to have a heavy Ti isotope signature.

The main objectives of the present study are to (1) determine the Ti isotopic composition of the major groups of chondrites and (2) analyze the Ti isotopic composition of a comprehensive set of terrestrial komatiites, howardite-eucrite-diogenite (HED) meteorites, aubrites, angrites, a martian shergottite and a lunar KREEP-rich impact melt breccia to constrain the igneous history of these planetary objects.

2 Samples

2.1 Komatiites

Komatiites are high-MgO volcanic rocks formed via high degrees of partial melting (*i.e.*, between 30 and 50%; Arndt, 1977) of the mantle. This type of melting regime commonly leads to almost complete removal of incompatible elements, such as Ti, from the source into the melt. Komatiites are therefore well suited to characterize the isotopic composition of the mantle and have been used previously for that purpose in studies of Mg, Fe, Mo, Ga and Ni isotope systematics (Dauphas et al., 2010; Greber et al., 2015; Kato et al., 2016; Gall et al., 2016). The

samples studied are komatiites from the 3.55 Ga Schapenburg Greenstone Remnant (6 samples), the 3.48 Ga Komati (5) and the 3.26 Ga Weltevreden (6) Formations of the Barberton Greenstone Belt, the 2.72 Ga Alexo locality in the Abitibi Greenstone Belt (4) and the 2.7 Ga Reliance Formation of the Belingwe Greenstone Belt (5). Details of the petrology and geochemistry of the samples studied can be found in Puchtel et al., (2013) and Puchtel et al., (2014) for the Komati and Weltevreden systems, in Puchtel et al. (2016) for the Schapenburg system, in Puchtel et al. (2009) for the Belingwe samples and in Lahaye and Arndt (1996) and Dauphas et al. (2010) for the Alexo system.

2.2 Meteorites

Titanium isotopic compositions were measured in 15 chondrites, 11 achondrites from the howardite-eucrite-diogenite (HED) clan, 6 aubrites, 5 angrites, a martian shergottite, and one lunar KREEP meteorite sample. The analyzed chondrites include meteorites from the H (Ste Marguerite, Queen's Mercy, Pultusk), L (Bald Mountain, Farmington), LL (Kelly, Dhurmsala, Chelyabinsk), EH (Sahara 97072), EL (Blithfield, Pillistfer), CO (Lancé), CM (Murray), CI (Orgueil) and CV (Allende) groups. All chondrites, except Kelly, Sahara 97072 and Blithfield, are observed falls. The Allende sample is a powder aliquot from the Smithsonian Allende standard (4 kg of homogenized and milled sample material, see Jarosewich et al. 1987), which should provide a good estimate of the composition of Allende unaffected by nugget effects associated with the presence of large CAIs (Davis et al., 2016).

The HED-clan meteorites represent the best crustal samples from a differentiated asteroid; most likely Vesta (Consolmagno and Drake 1977). They sampled lower crustal rocks (diogenites), gabbroic rocks formed within the crust (cumulate eucrites), shallow level rocks such as sills and lava flows (basaltic eucrites) and breccias consisting of a mixture of eucrite and diogenite (howardites) (e.g. Mandler and Elkins-Tanton 2013; Mittlefehldt 2015). We analyzed two diogenites (Johnstown, Tatahouine), one howardite (Kapoeta), two cumulate eucrites (Serra de Magé, Nagaria) and six basaltic eucrites for their Ti isotopic compositions. Except for Camel Donga, all HED-meteorites are falls. Basaltic eucrites can be further subdivided into three groups based on their chemical compositions. Using the terminology of Mittlefehldt (2015), the samples studied cover all three basaltic eucrite subgroups, namely, the Stannern-group (Stannern), the Nuevo-Laredo group (Lakangaon), and the main-group (Millbillillie, Camel Donga, Juvinas). Ibitira is an unusual eucrite, as it has a distinct oxygen isotopic composition (Wiechert et al., 2004), alkali element content and Ti/Hf ratio (Mittlefehldt 2005) compared to other HED meteorites. It plots, however, together with other HEDs in the ^{53}Mn-^{53}Cr (Lugmair and Shukolyukov 1998; Trinquier et al., 2008) and ^{60}Fe-^{60}Ni (Tang and Dauphas 2012) isochron diagrams. It is thus unclear whether this sample comes from a distinct parent-body than other HEDs (Wiechert et al., 2004; Mittlefehldt 2005) or a mantle reservoir in Vesta that was never fully homogenized with the rest of the mantle (Dauphas and Schauble 2016).

Angrites are uncommon achondrites as they are enriched in refractory elements, such as Ca and Ti and depleted in volatile elements such as Na, K or Rb (Keil 2012). Based on their texture and mineralogy, they are divided into slowly cooled plutonic and rapidly cooled volcanic angrites. They consist mainly of anorthite, calcic olivine and Al-Ti bearing pyroxenes and contain as accessory phases Ti-rich oxides such as ulvöspinel, titanomagnetite and ilmenite. We analyzed the δ^{49}Ti of two plutonic (NWA 4590 and NWA 2999) and three volcanic angrites (D'Orbigny, NWA 1670 and Sahara 99555). All analyzed angrites are finds.

Aubrites are unusual achondrites, likely due to the fact that core-mantle differentiation and magmatic evolution on their parent-body occurred under highly reducing conditions (Watters and Prinz 1979; Okada et al., 1988; Keil 1989). They consist mostly of FeO-free enstatite. Many normally lithophile elements, including Ti, Mn and Ca, exhibit chalcophile behavior (Watters and Prinz 1979). Due to the very similar O (Clayton and Mayeda, 1996), Ni (Tang and Dauphas 2012), Ti (Zhang et al., 2012), Ca (Dauphas et al., 2014a) and Cr (Trinquier et al., 2007) isotopic anomalies to those measured in enstatite chondrites, and their strongly reduced nature, aubrites are usually thought to have evolved from an enstatite chondrite-like precursor (Keil et al., 2010). The studied aubrites include the observed falls, Bishopville, Cumberland Falls, Norton County, Peña Blanca Spring, Bustee, and the find Shallowater, which has a distinct metal content compared to other aubrites and a complex and unique three stage cooling history, suggesting that it was derived from a distinct parent-body (Keil et al., 1989).

Martian meteorite NWA 11115 is a REE enriched basaltic shergottite, found in Morocco in 2016. Abundant secondary calcite indicates that NWA 11115 suffered from terrestrial alteration (Daswani et al., 2017).

The lunar KREEP sample analyzed for δ^{49}Ti is an aliquot of the matrix of the impact melt breccia of meteorite Sayh al Uhaymir (SaU) 169. KREEP is an acronym for lunar material that is highly enriched in K, REE, P and other incompatible trace elements (Warren and Wasson 1979). SaU 169 is the sample that shows the strongest enrichment in KREEP components known to date and was formed by impact melting of pre-existing KREEP-materials at 3.9 Ga (Gnos et al., 2004; Korotev 2005; Lin et al. 2012). The mineralogy of the melt breccia matrix is dominated by Ca-poor pyroxene, plagioclase and ilmenite with accessory zircon and phosphates.

3 Methods

All the meteoritic and Alexo komatiite sample powders were produced using agate mortar and pestle. Details of the sample preparation techniques for the Schapenburg, Komati, Belingwe and Weltevreden komatiites are reported in Puchtel et al. (2016), Puchtel et al. (2013) and Puchtel et al. (2009). In contrast to previous studies that analyzed Ti isotopes by MC-ICP-MS (e.g. Millet et al., 2014, Williams 2014, Zhang et al., 2011, Trinquier et al., 2009, Leya et al., 2008), samples for this work have been digested using alkali flux fusion. Alkali flux fusion with lithium metaborate ($LiBO_2$) is advantageous as (i) it affords complete dissolution of refractory accessory minerals, (ii) it avoids the creation of insoluble Ti-bearing fluoride that may cause mass-dependent Ti isotope fractionation, (iii) glass pellets are digested in HNO_3 avoiding the use of HF and $HClO_4$ and (iv) boron in the flux prevents fluorine in lab fumes to complex with Ti and, thus, ensures that Ti partitioning behavior on the ion-exchange chromatography columns is as expected. The flux fusion technique applied followed the protocol described in Pourmand et al. (2012), with some modifications. Sample powder and $LiBO_2$ were mixed in the proportions 1:6 and transferred to high purity graphite crucibles. Around 20 mg of a high-purity LiBr non-wetting solution was added per 100 mg of sample-flux mixture. The sample-flux mixture was subsequently fused in a furnace at 1,100°C for approximately 10 minutes. After the charge cooled, it was removed from the graphite crucible with tweezers and broken into pieces in a mortar. Afterwards, clean glass pellet pieces were separated by hand from those that were contaminated with graphite from the graphite crucible. Several millimeter-size clean glass fragments containing more than ~2 μg total Ti were transferred to Savillex PFA beakers, spiked with a ^{47}Ti-^{49}Ti double spike and digested in 10 mL of 3 M HNO_3 on a hot plate set at 130 °C, with repeated treatment in an ultrasonic bath. The amount of double-spike added was calculated based on the known sample Ti concentration and mass, and the fragment mass. For some low-Ti aubrites, the total Ti in the fragment was around 1 μg. The sample solution was subsequently evaporated and re-digested at 150 °C in 12 M HNO_3. Titanium was purified following the two-step ion-exchange chromatography protocol outlined in Millet et al. (2014) and Zhang et al. (2011). During the first step, Ti was separated from the matrix on a 2 mL Eichrom TODGA column, and during the second step, the Ti fraction was purified using a 0.8 mL AG1-X8 Bio-Rad column. The second step is primarily used to remove molybdenum, whose doubly charged ions can interfere with Ti isotopes (Zhang et al. 2011). The second step was repeated twice. In each batch of ~15 samples, at least one of the USGS standard reference material, such as G3, BIR-1a or BHVO-2, was added as unknown.

Blank levels were evaluated by measuring the Ti concentration by isotope dilution of fluxed $LiBO_2$ that was subsequently treated in a similar manner as the samples. As the $LiBO_2$ flux is the predominant blank source, the blank contribution to the sample is defined by the flux to sample ratio, i.e. 6:1. For 45 mg of melted and processed flux, which is higher than the amount of pellet sample aliquot used, the blank Ti amount is 18 ng, which constitutes <0.5% of the total Ti present in the samples, except for some low-Ti aubrites (i.e. Shallowater, Cumberland Falls and Peña Blanca Spring), where the total analytical blank contribution was up to 2%.

The Ti isotopic composition was analyzed using a Neptune MC-ICP-MS at the University of Chicago, measuring simultaneously Ti isotopes at masses 46, 47, 48, 49, and 50, as well as ^{44}Ca for correction of the interferences from ^{46}Ca and ^{48}Ca on ^{46}Ti and ^{48}Ti, respectively. Several of the analyzed isotopes suffer from polyatomic interferences: ^{44}Ca ($^{14}N_2{}^{16}O$, $^{28}Si^{16}O$), ^{46}Ti ($^{30}Si^{16}O$), and ^{50}Ti ($^{36}Ar^{14}N$). The measurements were therefore performed in high-resolution mode on the peak shoulder at a mass below the $^{36}Ar^{14}N$ interference on ^{50}Ti, thus avoiding polyatomic interferences. The ^{46}Ca and ^{48}Ca interferences were corrected for each cycle using the exponential mass fractionation law,

$$^{i}Ca = {}^{44}Ca_{measured} \cdot R_{Natural}^{{}^{i}Ca/{}^{44}Ca} \cdot (m\ {}_{{}^{i}Ca}/m_{{}^{44}Ca})^{\beta}$$

where $R_{Natural}$ is the natural abundance ratio after IUPAC, m is the mass of the isotope and β is the lab-

induced fractionation factor that is calculated from the double spike reduction individually for each measurement. The Neptune instrument was upgraded with an OnToolBooster jet pump for the interface and X skimmer and Jet sampler cones were used. The Ti isotopic composition for each sample is reported in δ^{49}Ti notation, which is the per mil deviation from the ^{49}Ti/^{47}Ti ratio of the Origins Laboratory Ti standard (OL-Ti) used in previous studies (the notation adopts the recommendations of Teng et al., 2017):

$$\delta^{49}Ti\ (‰) = \left[\frac{\left(^{49}Ti/^{47}Ti\right)_{Sample}}{\left(^{49}Ti/^{47}Ti\right)_{Ol\text{-}Ti}} \text{-}1\right] * 1000.$$

Isotope mass fractionation during Ti purification and ICP-MS measurements was monitored and corrected for using the double-spike technique. Titanium-50 was not used in the double spike data reduction, as it suffers from ^{50}Cr and ^{50}V interferences and is also affected by the largest mass-independent Ti isotope anomalies (Zhang et al., 2012, Leya et al., 2008, Trinquier et a., 2009). Details of the ^{47}Ti-^{49}Ti double spike and the OL-Ti calibration and instrument setup are described in Millet et al. (2014). Briefly, samples and standards were measured in 0.3M HNO_3 + 0.005M HF and introduced into the mass spectrometer using an Apex HF or an Aridus I desolvating nebulizer system. The Ti isotopic compositions and measurement precisions are identical for the two introduction systems used. Each sample measurement was bracketed by measurements of the standards with ^{48}Ti concentrations matched to within ± 10%. After a block of six to eight samples, a clean solution, prepared from the same batches of acids used for preparing the standard and sample solutions, was measured and used for on-peak zero baseline correction.

The uncertainty on the Ti isotopic compositions has been evaluated according to Dauphas et al., (2009) and encompasses within-session as well as long term external reproducibility. The uncertainty is assumed to be the combination of the internal error ($\sigma_{\mathrm{MassSpec}}$; commonly around ± 0.008 ‰), corresponding to repeated measurements of a single Ti solution and unknown errors ($\sigma_{\mathrm{Unknown}}$), for example isotopic fractionation prior to spike-sample equilibration. The value of $\sigma_{\mathrm{Unknown}}$ was assessed by examining the long-term external reproducibility (± 0.013 ‰; from rock digestion to isotopic analysis) of three different geostandards (G3, BHVO-2 and BIR-1a). The total uncertainty on a measurement is then defined as $e_{\mathrm{Data}} = 2 \cdot \sqrt{\sigma^2_{\mathrm{Unknown}} + \sigma^2_{\mathrm{MassSpec}}}$, with e_{Data} being the 95% c.i. (Dauphas et al., 2009).

Extraterrestrial samples, however, suffer from isotope anomalies on ^{46}Ti and ^{48}Ti and to obtain purely mass-dependent Ti isotope variations, one must correct for these anomalies. This correction is further explained in section 3.2; as a result of the corrections, the uncertainty on the δ^{49}Ti for extraterrestrial samples is estimated to increase up to ±0.042 ‰.

3.1 Test of the accuracy

One potential difficulty of using flux fusion samples to analyze Ti isotopes is that Li could theoretically cause ArLi molecular interferences on masses ^{46}Ti and ^{47}Ti. Even though mass scans over the masses of Li of samples and blanks were identical and did not indicate the presence of Li, several tests were performed to check if the newly developed digestion technique resulted in accurate outcomes.

(i) As first test, BIR-1a and BHVO-2, as well as four komatiite samples, were prepared following the methodology (i.e., conventional acid attack digestion) described in Millet et al. (2014) (labeled with the suffix “acid”, as in “BIR-1a acid” in Appendix Table B.1). The total Ti blank for the acid attack method was ≤10 ng.

(ii) The second test used matrix cuts of the first-step of column chemistry of three fluxed samples (M712, BV05 and 501-2) mixed with spiked standards as samples (labeled with the suffix “Matrix doped”, as in M712 Matrix doped in appendix Table B.1).

(iii) The third test used pure fluxed $LiBO_2$ mixed with double spiked OL-Ti standard (Flux Blank doped).

(iv) The fourth test was conducted by adding the Ti double-spike to the sample powder-flux mixture of ordinary chondrite sample Chelyabinsk prior to flux fusion (for other samples, the double-spike is added when a fragment of the solidified flux-sample melt is digested).

The Ti isotopic compositions of the four tests are shown in Table 1 and Appendix Table B.1. The first test resulted in identical δ^{49}Ti values, independent of the digestion technique applied. In addition, BIR-1a and BHVO-2 have the same Ti isotopic compositions as those reported in Millet et al. (2014). The matrix cuts and pure $LiBO_2$ samples mixed with spiked standard from tests (ii) and (iii) exhibit, as expected, a

δ^{49}Ti value that is within error of 0 ‰. The fourth test (iv) gave an identical δ^{49}Ti value for the two aliquots of Chelyabinsk, irrespective of when the Ti double-spike was added. Thus, the performed tests indicate that the change in the analytical technique involving flux fusion rather than acid digestion yields accurate Ti isotopic data.

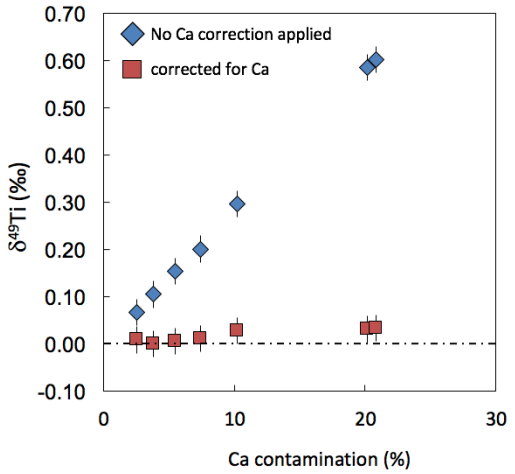

Figure 1: Titanium isotopic compositions of Ca doping experiment of data left uncorrected (blue diamonds) and data corrected for Ca interference on ^{46}Ti and ^{48}Ti (red squares). Measurements can be made on solutions that contain up to 20 wt.% Ca, while the samples measured in this study have Ca at a level of less than 5 wt.%.

To evaluate the accuracy and effectiveness of our correction of Ca isotope interference on ^{46}Ti and ^{48}Ti, Ca doping tests were performed, where different amounts of Ca were added to the spiked OL-Ti standard. The percent of Ca relative to Ti ranged from 3% to 21% (Fig. 1 and appendix Table C.2). As evident from Fig. 1, if no Ca correction is applied, the Ti isotopic composition increases linearly with the Ca/Ti ratio, reaching a δ^{49}Ti value of +0.6 ‰ at 20% Ca contamination. However, when the Ca correction is applied, samples with ≤ 10% Ca do not show any significant departure from the standard value (i.e., 0‰). At around 20% Ca contamination, the δ^{49}Ti value increases just slightly outside our measurement precision of ± 0.03 ‰. Most samples measured contained less than 1% Ca and no sample had more than 5% Ca. Thus, we conclude that any Ca interference present was adequately corrected for.

An additional test was performed to determine the efficiency with which Ti was purified during each of the different ion-exchange chromatography steps. From each of the three reference materials BHVO-2, BIR-1a and G3, an aliquot of the sample solution was taken after each ion-exchange chromatography step, named cut1, cut2 and cut3. For all three reference materials, the δ^{49}Ti value obtained for different cuts were identical within uncertainty, meaning that the level of purity of the final solutions exceeded the requirements to achieve accurate Ti isotopic measurements.

3.2 Data reduction and correction for Ti isotope anomalies

The Ti isotope data reduction was done in Mathematica following the method outlined in Millet et al. (2014) and Tissot et al. (2015). A complication arises with meteorites in that some isotopes are affected by the presence of nucleosynthetic anomalies. When no such anomalies are present, the ratio in the sample is assumed to be related to that of a standard by the laws of mass-dependent fractionation (an exponential law is often assumed), so we have $R^{i/j}_{sample} = R^{i/j}_{Standard} \cdot (m_i/m_j)^{\alpha}$. If isotopic anomalies are present (noted $\varepsilon^{i/j}_{Measured}$), this assumption is not warranted and the formula is modified accordingly (see Appendix A for details),

$$R^{i/j}_{Measured} = \left[p \cdot R^{i/j}_{Spike} + (1-p) \cdot R^{i/j}_{Standard} \cdot \left(\frac{m_i}{m_j}\right)^{\alpha} \cdot e^{\varepsilon^{i/j}_{Measured}/10^4}\right] \cdot \left(\frac{m_i}{m_j}\right)^{\beta}$$

where $R^{i/j}_{Measured}$, $R^{i/j}_{Standard}$ and $R^{i/j}_{Spike}$ are the ratios of the measured sample, the standard and spike; m_i and m_j are the masses of isotopes i and j and, p is the proportion of isotope j in the sample-spike mixture, α is the extent of natural mass fractionation, β corresponds to lab-induced isotopic fractionation, and $\varepsilon^{i/j}_{Measured}$ denotes isotopic anomalies (departure in part per 10,000 relative to terrestrial composition) measured by internal normalization by fixing the ^{49}Ti/^{47}Ti ratio constant to correct for natural and lab-induced isotopic mass fractionation. This equation has three unknowns; p, α and β. To solve it, three independent equations are written using the three isotopic ratios ^{46}Ti/^{47}Ti, ^{48}Ti/^{47}Ti and ^{49}Ti/^{47}Ti.

Average ε^{46}Ti and ε^{48}Ti data published in Zhang et al., (2012) and Trinquier et al., (2009) were used for correcting the mass-dependent Ti isotopic compositions of ordinary chondrites (ε^{46}Ti = -0.08 ± 0.01; ε^{48}Ti = -0.02 ± 0.12), enstatite chondrites (ε^{46}Ti = 0.01 ± 0.02; ε^{48}Ti = -0.02 ± 0.06), HED meteorites (ε^{46}Ti = -0.22 ± 0.03; ε^{48}Ti = -0.05 ± 0.06), angrites (ε^{46}Ti = -0.21 ± 0.04; ε^{48}Ti = 0.06 ± 0.20), aubrites

(ε^{46}Ti = 0.01 ± 0.03; ε^{48}Ti = -0.05 ± 0.16) and martian shergottite NWA 1115 (ε^{46}Ti = -0.17 ± 0.04; ε^{48}Ti = -0.07 ± 0.07), while individual meteorite ε^{46}Ti and ε^{48}Ti data were used for correcting δ^{49}Ti of carbonaceous chondrites. The Moon and aubrite parent-body have the same ε^{46}Ti and ε^{48}Ti as the Earth (Zhang et al., 2012). Aubrites and lunar soil samples can have high exposure ages and thus, the Ti isotopic composition might be affected by cosmogenic effects. The impact on ε^{46}Ti and ε^{48}Ti due to cosmogenic effects is, however, 2 to 4 times lower than for ε^{50}Ti, and both, aubrites and lunar meteorites have identical or almost identical ε^{46}Ti, ε^{48}Ti and ε^{50}Ti as the Earth (see appendix of Zhang et al., 2012). Because we do not use ^{50}Ti for our double spike reduction, the impact on the mass-dependent Ti isotopic composition of cosmogenic effects for these meteorite groups is insignificant given the current measurement precision.

The additional error on the δ^{49}Ti value arising from the correction of isotope anomalies was estimated using a Monte Carlo approach (n = 10,000 simulations) by generating normally distributed ε^{46}Ti and ε^{48}Ti values with the mean and error of each meteorite. The uncertainty resulting from the correction for Ti isotope anomalies ranges from ±0.007 ‰ for enstatite chondrites to ±0.024 ‰ for angrites. The total error (95% c.i.) on the δ^{49}Ti was then calculated as $e_{Total} = \sqrt{e^2_{Anomalies} + e^2_{Data}}$.

3.3 *Recommended data representation of titanium isotopic compositions*

To facilitate inter-laboratory comparison of Ti isotope data, we recommend that δ^{49}Ti data is published normalized to the Origins Laboratory Ti standard (OL-Ti), which can be requested at SARM (Service d'Analyses des Roches et des Minéraux, Nancy, France). The OL-Ti standard fulfills the guidelines for a suitable reference material as put forward by Teng et al., (2017). It also has an ideal Ti isotopic composition, which is within current measurement precision identical to the bulk silicate Earth (Millet et al., 2016). The δ^{49}Ti value of NIST SRM 3162a relative to OL-Ti is +1.056 ± 0.026 ‰ (Table B.1). If in-house Ti reference materials other than the OL-Ti standard are used, it is suggested to calibrate them against the OL-Ti standard and to subsequently correct the δ^{49}Ti data for the offset between the two Ti reference materials. For example, δ^{49}Ti data measured relative to standard reference material 3162a from NIST can be recalculated to the OL-Ti standard with $\delta^{49}Ti_{OL\text{-}Ti} = \delta^{49}Ti_{SRM3162a} + 1.056‰$.

4 Results

The Ti isotopic compositions of various terrestrial and extraterrestrial materials analyzed in this study are presented in Tables 1 to 3. Unless otherwise stated, all uncertainties are given as 95% confidence intervals (c.i. hereafter). No significant variation is found in the Ti isotopic composition of chondrites, except possibly for a slightly heavier δ^{49}Ti value in the Allende CV chondrite. The heavy δ^{49}Ti value of Allende is presumably due to the large modal fraction of refractory dust in this sample relative to other chondrites (Hezel et al. 2008, Dauphas and Pourmand 2015). Excluding this sample, chondrites define a mean δ^{49}Ti value of +0.004 ± 0.010 ‰, which is in excellent agreement with the proposed composition of the bulk silicate Earth (Fig. 2 and Table 1; Millet et al., 2016). The very consistent δ^{49}Ti observed among all investigated chondrite groups is in contrast to the isotope pattern of the similarly refractory and lithophile Ca, where carbonaceous chondrites have lighter δ^{44}Ca than enstatite and ordinary chondrites (Fig. 3; Simon and DePaolo 2010; Valdes et al., 2014).

The range in δ^{49}Ti values of komatiites is similar to that observed among post-Archean mafic and ultramafic rocks (Millet et la., 2016). Individual samples from the Schapenburg, Komati, Belingwe and Alexo komatiites are within error identical and define average Ti isotopic compositions of +0.025 ± 0.020 ‰, +0.002 ± 0.024 ‰, +0.016 ± 0.012 ‰ and -0.035 ± 0.016 ‰, respectively. In the Weltevreden system, measurements of samples 501-1, 501-8 were shifted towards lighter δ^{49}Ti values (-0.072 ± 0.030 ‰ and -0.102 ± 0.030 ‰, respectively) compared to the other samples from that locality. Replicate analyses of newly prepared aliquots from the fluxed pellets of samples 501-1 and 501-8 yielded δ^{49}Ti values of +0.004 ± 0.033 ‰ and -0.001 ± 0.033 ‰, respectively, which are identical within errors to the rest of the Weltevreden samples. It is likely that the light δ^{49}Ti compositions from the first measurements of samples 501-1 and 501-8 from Weltevreden are incorrect. The calculated Ti concentrations with isotope dilution for these two samples resulted in around 12% higher Ti concentrations for the second measurement. This could indicate that an error occurred during the spiking procedure or the spike-sample mixture did not completely equilibrate. Excluding the two light outliers, the average δ^{49}Ti of the Weltevreden komatiites is -0.015 ± 0.012 ‰. Therefore, no correlation be-

tween age and the Ti isotopic compositions of komatiites is observed. The overall average Ti isotopic composition of all komatiites (i.e., δ^{49}Ti = -0.001 ± 0.019 ‰) is identical within uncertainties to the bulk silicate Earth δ^{49}Ti value of +0.005 ± 0.005 ‰ reported by Millet et al. (2016).

The δ^{49}Ti values of the HED meteorites studied vary between -0.04 and +0.04 ‰ and thus span a similar range as that observed for terrestrial basalts (Millet et al., 2016). No difference in the Ti isotopic composition of diogenites, howardites and eucrites is observed and the overall average δ^{49}Ti is +0.011 ± 0.015 ‰. Four out of the five studied angrites have a Ti isotopic composition similar to chondrites, with values ranging from -0.010 ± 0.042 to +0.042 ± 0.042 ‰. Plutonic angrite NWA 4590 has a significantly lighter δ^{49}Ti of -0.111 ± 0.042 ‰. No systematic difference in the Ti isotopic composition can be observed between volcanic and plutonic angrites and no correlation between the Ti isotopic composition and major or trace element concentrations of angrites exists, except that the sample most enriched in TiO_2 (NWA 4590 = 1.42 wt%; Shirai et al., 2009, Keil 2012) has the lightest δ^{49}Ti. The martian shergottite has a δ^{49}Ti value of +0.021 ± 0.038 ‰, consistent with the Ti isotopic composition of chondrites.

The variation in the Ti isotopic composition among aubrites is over 0.30 ‰ (Table 3) and, thus, is much higher than what is observed in terrestrial basalts and HED meteorites. Bishopville and Northon County have the heaviest (+0.242 ± 0.034 ‰) and lightest (-0.069 ± 0.034 ‰) δ^{49}Ti values, respectively. The δ^{49}Ti of aubrites correlates negatively with MgO concentration and MgO/SiO_2 ratio. Shallowater, an aubrite with a proposed distinct parent-body (Keil 1989), has a δ^{49}Ti value of +0.065 ± 0.034 ‰ and plots outside of the Ti isotopic composition *vs.* MgO trend defined by the other aubrites.

Finally, lunar KREEP sample SaU 169 has a composition highly enriched in heavy Ti isotopes (+0.330 ± 0.034 ‰), a signature that is well resolvable from the δ^{49}Ti values of low-Ti and high-Ti mare basalts (ranging from -0.008 to +0.033 ‰), as reported by Millet et al., (2016).

5 Discussion

5.1 Titanium isotope composition of chondrites and comparison with calcium isotopes

The Ti isotopic compositions of ordinary, enstatite, and carbonaceous chondrites are identical within their respective uncertainties (Fig. 2) and define an average of +0.004 ± 0.010 ‰. This observation contrasts with the documented isotope heterogeneity in Ca isotopes among chondrites (Fig. 3; refs). Calcium is slightly less refractory than Ti but both have high 50% condensation temperature of 1517 and 1582 K, respectively (at 10^{-4} bar total pressure in a gas of solar composition) (Grossman and Larimer 1974; Lodders 2003). Both Ca and Ti are lithophile and do not partition in either metal or sulfide except under highly re-

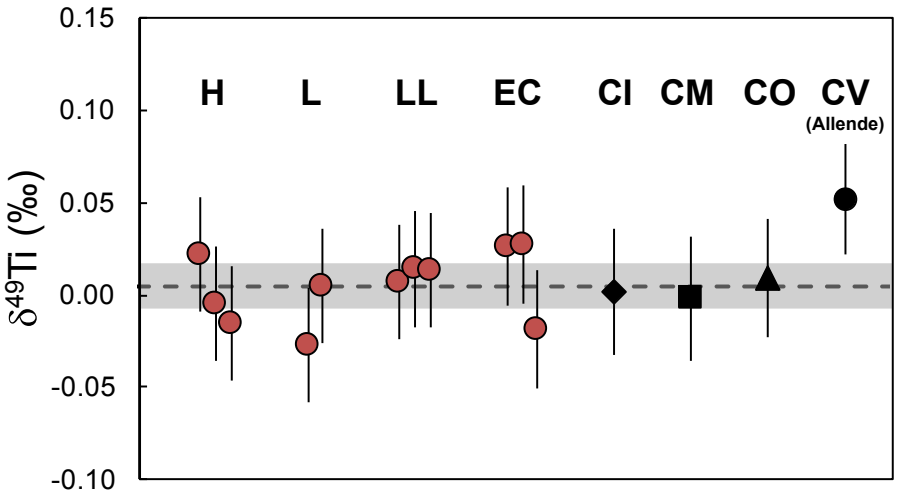

Figure 2: Titanium isotope compositions of ordinary, enstatite and carbonaceous chondrites. The shaded area shows the average δ^{49}Ti value (± 95% c.i.) of measured chondrites; +0.004 ± 0.010‰ (CV chondrite Allende not included, see text).

ducing condition. One might thus expect that isotopic variations of Ti would mirror those documented for Ca. However, unlike δ^{49}Ti, the calcium isotope compositions (δ^{44}Ca) of most carbonaceous chondrites, except those of the CO group, are lighter than that of the bulk silicate Earth, ordinary and enstatite chondrites (Simon and DePaolo 2010, Valdes et al., 2014, Huang and Jacobsen 2017). The reason for the δ^{44}Ca variation among carbonaceous chondrites is not yet well understood. Recently, it was suggested that the light Ca isotopic composition of carbonaceous chondrites may be linked to the amount of incorporated calcium-aluminum rich inclusions (CAI) and refractory dust (Dauphas and Pourmand 2015, Huang and Jacobsen 2017). CAIs are among the earliest solar nebula condensates and, as a result of kinetically driven isotope fractionation during condensation and/or evaporation (Huang et al., 2012), they carry a very light Ca isotope signature, reaching -11 ‰ (Niederer and Papanastassiou 1984; Huang et al., 2012; Simon et al., 2016a). The high Ca concentration and low δ^{44}Ca value of refractory dust can influence the Ca budget and isotopic composition of chondrites. This idea is corroborated by the REE signature of carbonaceous chondrites, where the presence of an extraneous CAI/refractory dust component is manifested as a Tm excess relative to other meteorite groups, Earth, Mars, and Vesta (Dauphas and Pourmand 2015; Barrat et al., 2016). An important difference between Ca and Ti in CAIs is that while Ca isotopes show overall light composition, Ti isotopes show variations that are centered on the chondritic composition (Davis et al., 2016; Simon et al., 2016a). The effect on the Ti and Ca isotope compositions of mixing a CAI/refractory component with an ordinary chondrite was calculated using published Ca and Ti isotopic compositions and concentrations. For the Ca and Ti concentrations of the refractory dust, the suggested average values for type II CAIs by Dauphas and Pourmand (2015) are used (i.e. Ti = 4065 μg/g; Ca = 8.4 wt.%). For the Ca and Ti isotopic compositions, the average δ^{44}Ca of type II CAIs from Huang et al. (2012) and the average δ^{49}Ti of CAIs from Zhang (2012) are used (δ^{44}Ca = -3.64 ‰ and δ^{49}Ti = 0.22 ‰). The Ca and Ti concentrations of ordinary chondrites are 1.29 wt.% and 617 μg/g, respectively (Wasson and Kallemeyn 1988). As shown in Fig. 3, mass balance predicts that mixing 2% of a CAI component in ordinary chondrites will lower their δ^{44}Ca by around -0.54 ‰ but will have little effect on their δ^{49}Ti (i.e. +0.026 ‰).

The reason why the Ti and Ca isotope systems are decoupled in early refractory solar nebula condensates is not yet well understood. One reason for

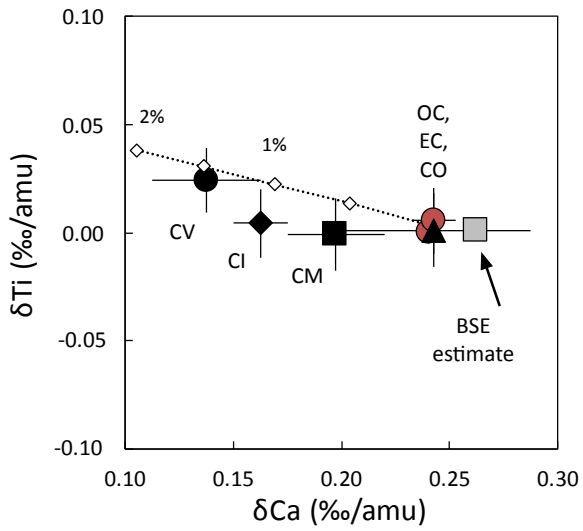

Figure 3: Average Ti isotopic composition versus Ca isotopic composition of various chondrite groups (OC, EC, CO, CM, CI and CV) and the bulk silicate Earth (BSE) in permil per atomic mass unit [δTi=δ^{49}Ti/(49-47) and δCa=δ^{44}Ca/(44-40)]. Ti isotope data is from this study (Table 1) and Ca isotope data from Valdes et al., (2014). Carbonaceous chondrites have a significantly lighter Ca isotopic composition than the Earth, ordinary and enstatite chondrites. In contrast, all chondrite groups have the same Ti isotopic composition within uncertainty. The dotted line with white diamonds is the mixing curve between an ordinary chondrite and refractory dust (CAIs) in 0.5% increments (see text for details). Because CAIs have on average chondritic Ti isotopic composition, their removal or addition does not affect the Ti isotopic composition of bulk meteorites significantly, which it does affect the Ca isotopic composition (see text for details).

the higher 50% condensation temperature of Ti relative to Ca is that Ti condenses as perovskite whose stoichiometry ($CaTiO_3$) dictates that for every Ti that condenses one atom of Ca also condenses. Because the Ca/Ti ratio of solar gas is ~25, only a small fraction is Ca is condensed when Ti is fully condensed in perovskite (Grossman and Larimer 1974). The fact that average Ti isotopic composition of CAIs is similar to that of chondrites, despite displaying a significant range in δ^{49}Ti values, suggests that CAIs as a whole behaved as a closed-system for Ti. Some CAIs were enriched in the light isotope by kinetic isotope fractionation associated with condensation from supersaturated gas but the isotopically heavy Ti left behind in the gas was eventually condensed in other CAIs and

no net loss of Ti from the CAI-forming region took place. Calcium on the other hand is slightly less refractory and is enriched in the light isotopes. Following condensation of isotopically light Ca, the residual isotopically heavy Ca gas was driven off from the CAI-forming region but Ti was already all in the solid, so its isotopic composition was unaffected. Further work on CAIs is needed to understand what caused the isotopic decoupling between Ca and Ti but their distinct condensation behaviors apparently affected the compositions of bulk chondrites.

5.2 Titanium isotope variability in terrestrial mafic and ultramafic rocks

As was discussed earlier, the average chondritic Ti isotopic composition of +0.004 ± 0.010 ‰ obtained in this study agrees well with the proposed value for the bulk silicate Earth (+0.005 ± 0.005 ‰; Millet et al., 2016), implying that the Earth has a chondritic δ^{49}Ti value. Titanium is a lithophile element, so the only mechanism that could have conceivably fractionated the isotopic composition of the Earth at a large scale, after its accretion, is continental crust extraction. Indeed, evolved crustal rocks have a heavier Ti isotopic composition than basalts or peridotites (Millet et al., 2016). However, Millet et al. (2016) did not observe significant Ti isotope fractionation during mantle melting processes and, thus, it is more likely that the isotopically light counterpart to the heavier upper continental crust is the lower continental crust. In addition, a first order calculation of the effect of crust extraction on the δ^{49}Ti of the terrestrial mantle indicates that this process is unlikely to change the Ti isotopic composition of the mantle. The average Ti concentration of the bulk silicate Earth is estimated to be ~1205 μg/g (McDonough and Sun 1995) and that of the average continental crust is ~4316 μg/g (Rudnick and Gao 2003). The mass of the continental crust is around 0.6 wt.% of that of the bulk silicate Earth (Helffrich and Wood 2001). Hence, around 2.2 wt.% of the total Ti in the bulk silicate Earth is stored in the continental crust. An estimate of the average continental crust δ^{49}Ti value can be obtained by interpolating the δ^{49}Ti vs. SiO_2 correlation from Millet et al. (2016) to 60.6 wt.% SiO_2, the estimated average SiO_2 concentration of the bulk continental crust after Rudnick and Gao (2003). This yields an average continental crust δ^{49}Ti value of +0.21 ‰. The mass-balance would therefore predict that the mantle should have been shifted by -0.005 ‰ by continental crust extraction. The effect of crustal extraction on the Ti isotopic composition of the depleted mantle depends on the mantle volume that was depleted. Mass balance calculations of K, U and Th suggest that around 50% of Earth's mantle is depleted (Helffrich and Wood 2001). If correct, the δ^{49}Ti of the depleted mantle would have been shifted by around -0.010 ‰ from the chondritic value. Crustal extraction therefore had little influence on the mantle Ti isotopic composition, consistent with the fact that terrestrial mafic and ultramafic rocks have Ti isotopic compositions similar to chondrites.

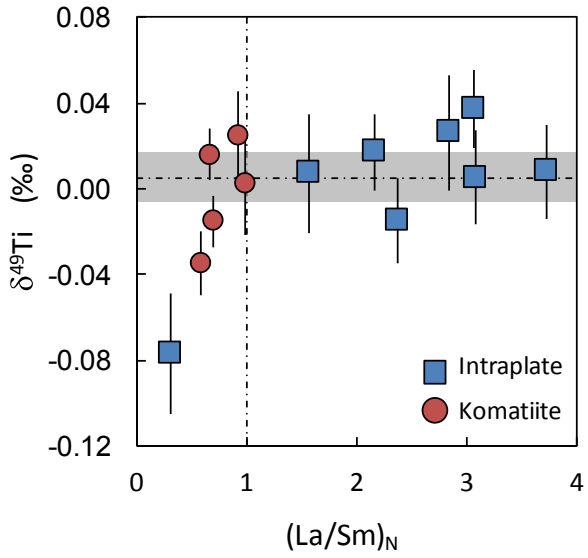

Figure 4: Titanium isotopic composition of intraplate basalts and komatiites versus chondrite normalized La/Sm ratios. The dashed lines correspond to the chondritic δ^{49}Ti and $(La/Sm)_N$ values. Samples with a subchondritic δ^{49}Ti values have the most depleted LREE patterns, indicating that they originate from a strongly depleted mantle source. The titanium isotopic data are from this study and Millet et al., (2016); REE data from Lahaye and Arndt (1996); Turner et al., (1997); Raczek et al., (2007); Millet et al., (2008); Millet et al., (2009); Puchtel et al., (2009); Puchtel et al., (2013); Puchtel et al., (2016); Fourny et al., (2016).

Komatiites have experienced extensive alteration. Titanium, which is highly insoluble in most aqueous fluids, was not mobilized by this alteration. Indeed, the TiO_2 concentration of the samples all plot on olivine control lines, meaning that Ti concentration variations in komatiites are entirely explainable by magmatic processes (see Puchtel et al., 2009, Puchtel et al., 2013, Puchtel et al., 2016 and Appendix Fig. C1). Among komatiites, one needs to distinguish between the bulk Ti isotopic composition of a lava flow and individual samples. The δ^{49}Ti of the latter might

have been affected by isotope fractionation induced by fractional crystallization after lava emplacement. For Komati, Weltevreden, Belingwe and Alexo komatiite lava flows, we analyzed olivine cumulates and spinifex textured rocks, which represent end members of *in situ* lava differentiation. However, no systematic difference in the Ti isotopic composition between olivine cumulates and spinifex textured rocks is observed. Also, the analyzed Schapenburg samples are identical within error, with the caveat that only spinifex-textured rocks were analyzed. Therefore, the bulk lava δ^{49}Ti of a komatiite system is estimated using the average Ti isotopic compositions of the samples from the respective komatiite location (see Table 2). Based on these considerations, the Komati, Schapenburg, Weltevreden (excluding measurements 501-1 and 501-8 with unusual light δ^{49}Ti) and Belingwe suites have a chondritic δ^{49}Ti (average = +0.007 ± 0.011 ‰) and the Alexo komatiites a slightly subchondritic δ^{49}Ti of -0.035 ± 0.016 ‰ but this is at the limit of precision (Fig. 4). While the shift towards heavier Ti isotopic compositions in basalts can be explained by an early onset of Fe-Ti-oxide crystallization (Millet et al., 2016), the shift towards a lighter than chondritic Ti isotopic composition is more difficult to explain. Indeed, no mineral phase has yet been identified that preferentially incorporates heavy Ti isotopes, which would result in a melt enriched in light Ti isotopes. Mantle derived rocks with a subchondritic δ^{49}Ti have been identified in island-arc basalts (JB-2, δ^{49}Ti = -0.046 ± 0.009; Millet et al., 2016), ocean island basalts (BIR-1a) and the Alexo komatiites. As Ti behaves as an incompatible element, one possible mechanism that could affect its isotopic composition is extensive depletion of the mantle. In such a process, one would expect to observe the strongest effect on the δ^{49}Ti in the Ti residue corresponding to the strongly depleted mantle. REE behave as a coherent series of elements whose incompatibility during mantle melting decreases with increasing atomic number (Winter 2001). The REE pattern thus can be used to infer the fertility of their mantle source region (e.g. Robin-Popieul et al., 2012). A depleted LREE pattern, i.e. low La_N/Sm_N ratio, is diagnostic of rocks sourced from a mantle region that already experienced prior melt extraction. As shown in Fig. 4, BIR-1a and the Alexo komatiites have the most depleted chondrite normalized LREE pattern ($La_N/Sm_N \leq 0.59$) and the lightest δ^{49}Ti of the entire suite of komatiites and intraplate basalts.

If melting processes can affect the Ti isotopic composition of the mantle, then a mechanism is needed that extracts preferentially heavy Ti isotopes during mantle melting, leaving behind a residue enriched in light Ti isotopes. Titanium in mafic melts is predominantly in 5-fold, but also 4- and 6-fold coordinations are present (Farges et al., 1996; Farges and Brown, 1997). Titanium-bearing mantle minerals like pyroxene, garnet and spinel, preferentially incorporate 6-fold Ti in their structure (Waychunas, 1987; O'Neill and Navrotsky, 1983). The situation with olivine is more complex. While in anhydrous olivine, Ti^{4+} substitutes for Si^{4+} into tetrahedral sites, in the presence of water Ti enters in six-fold coordination as Ti-clinohumite-like point or planar defects (Berry et al., 2007; Hermann et al., 2007). Olivine is, however, not expected to be an important host for Ti in the mantle (McDonough et al., 1992; Green et al., 1994) and thus, from a mass balance point of view, should not significantly affect the Ti isotope signature. Because low coordination is usually associated with stiffer bonds and heavy isotope enrichment, one would predict that depleted mantle would be shifted towards light δ^{49}Ti (Millet et al., 2016; Schauble, 2004), consistent with the observed low δ^{49}Ti values in magmas from strongly depleted sources. Depleted sources are also more prone to metasomatism, which taking Fe isotope systematics as a guide, can produce light Ti isotope signatures in some contexts (Weyer and Ionov 2007). A possible scenario is that metasomatism of a depleted source by Ti-rich melts was accompanied by diffusion of Ti from the melt to the solid. Because light Ti isotopes diffuse faster than heavier ones (Richter et al., 2009 and references therein), the metasomatized solid would be expected to be enriched in the light Ti isotopes during such a re-fertilization event.

An open question is to what extent a mantle source needs to be depleted to become significantly biased in its Ti isotopic composition. As seen in Fig. 4 and published Ti isotope data on eclogites, peridotites and N-MORB data (Millet et al., 2016), many rocks exhibiting a depleted LREE pattern and thus derived from a depleted mantle source have a δ^{49}Ti identical within errors to the bulk silicate Earth. To more rigorously explain and address the occurrence of subchondritic δ^{49}Ti among terrestrial mafic and ultramafic rocks, more data describing the Ti isotopic composition of important major minerals, such as garnet, pyroxene, spinel, and olivine, are needed. Studies targeting peridotites that have experienced re-fertilization and metasomatism should also help elucidate whether such processes can explain the light Ti isotope signature of depleted sources.

5.3 Titanium isotopic fractionation in aubrites

The variation in the Ti isotopic composition among aubrites is over 0.3 ‰ and is, thus, three times larger than what is observed for terrestrial basalts and HED meteorites. The δ^{49}Ti value of aubrites correlates well with their estimated MgO/SiO_2 ratio and the MgO concentration (compiled from the MetBase database), with the exception of Shallowater (Fig. 5). Shallowater has a distinct metal content compared to other aubrites and a complex and unique three stage cooling history, suggesting that it was derived from a distinct parent-body (Keil et al. 1989). Its outlier Ti isotopic composition relative to other aubrites further confirms the unusual nature of Shallowater in this meteorite group and consequently, it will be omitted from further discussion.

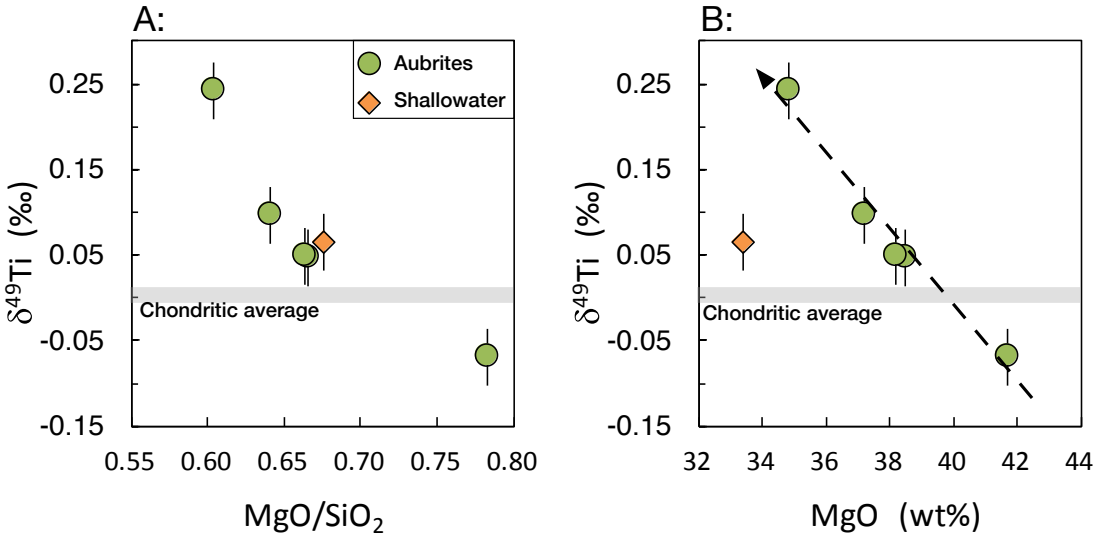

Figure 5: Titanium isotopic composition of aubrite meteorites as a function of MgO/SiO_2 ratio and MgO concentration. Shallowater, an aubrite from a distinct parent-body than the rest (Keil et al. 1989), plots outside of the δ^{49}Ti vs. MgO correlation defined by the other aubrites. The dashed arrow indicates the inferred direction of magmatic differentiation, interpreted to be due to redox isotopic fractionation between Ti^{3+} and Ti^{4+}, whereby crystallization leads to an enrichment of isotopically heavy Ti^{4+} in the melt. The horizontal grey bar represents the estimated chondritic Ti isotopic composition. The MgO and SiO_2 concentrations are compiled from the MetBase database.

The unusually large spread in δ^{49}Ti values in rocks with similar compositions is most probably the result of the very low fO_2 under which aubrite meteorites evolved. By analogy with enstatite chondrites, Ti likely exists in aubrites in the oxidation states Ti^{3+} and Ti^{4+} (Simon et al., 2016b), which favors a higher degree of isotope fractionation (Schauble 2004, Dauphas et al., 2014b). In these conditions, the nominally lithophile element Ti becomes chalcophile and is enriched in troilite (Watters and Prinz 1979). The TiO_2 concentration in aubritic meteorites is low, with values between 0.01 and 0.2 w.t% (Watters and Prinz 1979), a likely result of the removal of Ti from the mantle in a sulfide melt during core formation (Lodders et al., 1993). The good correlation between δ^{49}Ti and MgO/SiO_2 ratio and the MgO concentration, two indexes of magmatic differentiation, suggests that an igneous process, such as fractional crystallization or partial melting is responsible for the fractionated Ti isotopic composition. Partitioning of Ti between sulfide and silicate melt, as well as its presence in different oxidation states (Ti^{3+} *vs.* Ti^{4+}), are likely mechanisms to fractionate its isotopes in this reducing environment. Titanium-rich troilite is one of the major hosts of Ti in aubrites and most likely favors Ti^{3+} over Ti^{4+}. No data are yet available regarding the the partitioning behavior of Ti^{4+} *vs.* Ti^{3+} in silicate minerals from aubrites. In refractory inclusions, however, Ti^{3+} is preferentially incorporated into pyroxenes over Ti^{4+} and the melt from which they crystallize gets progressively depleted in Ti^{3+} and enriched in Ti^{4+} (Simon et al., 1991; Papike et al., 2016). Thus, sulfides and silicate minerals are expected to prefer Ti^{3+} over Ti^{4+} in their mineral structures, making it likely that with increasing fractionation of the system, the Ti^{4+}/Ti^{3+} ratio in the melt would increase. Following Schauble (2004) and Dauphas et al. (2014b), we can assume, as the first

order approximation, that species containing Ti^{4+} have a heavier Ti isotopic composition than those hosting Ti^{3+}. In addition, Ti-S bond length in Ti sulfides like TiS_2 (~2.4 Å; Chianelli et al.,1975) or heideite (~2.5 Å; Takahashi and Yamada, 1973) are longer than Ti-O bonds observed in silicate minerals like e.g. enstatite (~2.1 Å; Tarantino et al., 2002) or silicate glass (~1.9 Å; Cormier et al., 2001). The difference in bond length results in lower force constants of Ti-S bonds than in Ti-O bonds (Young et al., 2015). Weaker bonds favor light isotopes and thus, one can predict that sulfide minerals are enriched in light Ti isotopes. Therefore, silicates and sulfides should preferentially incorporate light Ti isotopes. Following this line of argument, increasing fractionation of the magmatic system should result in a progressively higher Ti^{4+}/Ti^{3+} ratio and thus a heavier δ^{49}Ti in the residual melt. This is consistent with the observed correlations between δ^{49}Ti and indices of magmatic differentiation.

Although there are still substantial gaps in our understanding of the geochemical behavior of Ti under these reducing conditions, the argument presented above at least qualitatively explains the observed δ^{49}Ti signatures in aubrites. The extraction of Ti from the mantle by a sulfide melt during core formation (Lodders et al., 1993) could have shifted the bulk silicate Ti isotopic composition of the aubrite parent-body towards a δ^{49}Ti value heavier than the chondritic average.

5.4 Titanium isotope fractionation in the lunar magma ocean

One of the remarkable features of lunar mare basalts is their highly variable and sometimes high Ti concentrations. One interpretation of this observation is that accumulated ilmenite from the latest stages of the lunar magma ocean crystallization (e.g. Snyder et al., 1992; Shearer and Papike 1999) was involved in the generation of high-Ti mare basalts (e.g. Wagner and Grove 1997; van Orman and Grove 2000). Following the argument of Millet et al., (2016) that the heavy Ti isotopic composition in evolved silicic crustal rocks on Earth is the result of light Ti isotopic fractionation into Fe-Ti oxides, the crystallization of ilmenite in the lunar magma ocean should have shifted the residual liquid towards a heavy Ti isotopic composition, too. Accordingly, KREEP-rich rocks (material that is highly enriched in K, REE, P and other incompatible trace elements) that represent the residual liquid from lunar magma ocean crystallization (Warren and Wasson 1979) may show enrichments in the heavy isotopes of titanium. The significantly distinct δ^{49}Ti value (+0.330 ± 0.034‰) of the KREEPy impact melt breccia part of SaU 169 therefore supports Ti isotope fractionation due to ilmenite crystallization in the lunar magma ocean. Following the Rayleigh distillation modelling approach of Millet et al., (2016) and using a Ti isotope fractionation value between melt and ilmenite of -0.118‰ (at T = 1125 °C; van Orman and Grove 2000), a δ^{49}Ti of +0.330‰ in the melt is achieved when approximately 94% of Ti has been removed in ilmenite (Fig. 6). At this point, the bulk ilmenite cumulate would have a δ^{49}Ti of -0.017‰ (Fig. 6).

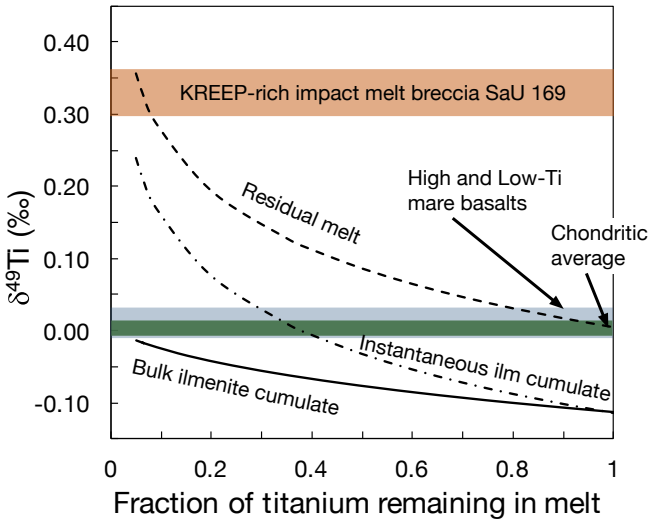

Figure 6: Evolution of the Ti isotopic composition of the lunar magma ocean and cumulate minerals after the onset of ilmenite crystallization, adopting the Rayleigh distillation modelling approach of Millet et al., (2016) and using a Ti isotopic fractionation value between melt and ilmenite of -0.118‰. The δ^{49}Ti value of KREEP-rich impact melt breccia SaU169 of +0.330‰ is achieved after 94% of Ti has been removed from the melt in ilmenite.

It is generally thought that the source of the high-Ti lunar mare basalts is linked to ilmenite-bearing cumulates, either by assimilation of ilmenite during magma ascent or by fertilization of ilmenite free mantle layers by sinking ilmenite-bearing cumulates or negatively buoyant partial melts from ilmenite-rich zones (e.g., Snyder et al., 1992; Wagner and Grove 1997; van Orman and Grove 2000; Elkins-Tanton et al., 2011; Hallis et al., 2014). However, high-Ti mare basalts have δ^{49}Ti ranging from +0.011 to +0.033‰ (Millet et al., 2016) and are thus heavier than the

estimated bulk ilmenite cumulate δ^{49}Ti of -0.017 ‰. This discrepancy suggests that either (i) preferentially late ilmenite cumulates which host a heavier δ^{49}Ti were the predominant Ti source of the high-Ti mare basalts, or (ii) that ilmenite was not exhausted during the melting process, so that significant fractionation was imparted to melt upon melting of the source of high-Ti mare basalts. The first option is somewhat *ad hoc* and difficult to test. The second process could have occurred during melting of ilmenite-bearing cumulates in the lunar mantle (Hess and Parmentier, 1995; Beard et al., 1998; Hallis et al., 2014) or during the production of a buoyant partial melt from an ilmenite-bearing layer that then subsequently sunk and fertilized parts of the lunar mantle with Ti (van Orman and Grove, 2000; Elkins-Tanton et al., 2004). It is currently not possible to evaluate which of the two latter processes was more likely to generate high-Ti mare basalts based on the Ti isotopic compositions of lunar rocks.

5.5 Titanium isotope signature of angrites, HED meteorites and Mars

The angrites NWA 2999, D'Orbigny, NWA 1670 and Sahara 99555 have Ti isotopic compositions that are identical within uncertainties. The average δ^{49}Ti value of these samples is +0.007 ± 0.038 ‰, which is indistinguishable from the chondritic value. Angrite NWA 4590, however, has a significantly lighter δ^{49}Ti of -0.111±0.042 ‰. Angrites are enriched in refractory elements, such as Ti and Ca, and thus contain minerals with high Ti concentrations, such as Al-Ti-rich diopside, ilmenite, magnetite and ulvöspinel (e.g. Keil 2012), which increases the possibility of Ti isotope fractionation via crystallization of these mineral phases. Published CaO and TiO_2 concentrations of angrites correlate well (appendix Fig. C.2), with exception of sample NWA 4590 that plots at a too high TiO_2 concentration relative to its CaO concentration, which likely is the result of the high abundance of ulvöspinel in that meteorite (~18 vol.%; Kuehner and Irving 2007). Angrite NWA 4590 has also an unusual coarse grained mineral texture that resembles cumulate rocks (Kuehner and Irving 2007). Assuming that (i) ulvöspinel is the major host of Ti in angrite NWA 4590 and thus defines its δ^{49}Ti composition and (ii) NWA 4590 equilibrated with a melt with chondritic δ^{49}Ti, then the Ti isotopic fractionation between the melt and ulvöspinel is approximately -0.115 ± 0.042 ‰. Such fractionation is consistent with the expected equilibrium fractionation between silicate melt and oxide of around -0.106 ‰ (Millet et al., 2016) assuming a crystallization temperature around the liquidus of a basaltic melt of ~1200°C. Therefore, the light δ^{49}Ti of NWA 4560 is likely the result of accumulation of ulvöspinel and is thus not representative of the bulk angrite parent-body. Consequently, the best estimate of the bulk angrite parent-body δ^{49}Ti is calculated as the average for angrites NWA 2999, D'Orbigny, NWA 1670 and Sahara 99555 only. This average δ^{49}Ti = +0.007 ± 0.038 ‰ is indistinguishable from the chondritic value.

A similar picture emerges from the analyzed HED meteorites. No systematic difference in the δ^{49}Ti values between diogenites, eucrites and howardites is observed and the overall average of +0.011 ± 0.015 ‰ is identical to the chondritic value. The similar Ti isotopic composition between diogenites (lower crust samples), cumulate eucrites (gabbroic rocks formed within the crust) and basaltic eucrites (sills and lava flows) (Mandler and Elkins-Tanton 2013; Mittlefehldt 2015) further indicates that Ti isotope fractionation in mafic systems is limited unless Ti exists in different oxidation states (as discussed for aubrites) or an Fe-Ti oxide like ilmenite reaches saturation (as discussed for the Moon).

The estimated Ti isotopic compositions of the parent-bodies of angrites (+0.007 ± 0.038 ‰) and HEDs (+0.011 ± 0.015 ‰), Mars (+0.021± 0.038 ‰; based on a single martian shergottite), the Moon (-0.003 ± 0.014 ‰; Millet et al., 2016) and the bulk silicate Earth (+0.005 ± 0.005 ‰; Millet et al., 2016), are all within error identical to the chondritic value of +0.004 ± 0.010 ‰, which argues for a widespread homogeneous δ^{49}Ti signature among solar system objects (Fig. 7 and Table 4).

5.6 Comparison with previously published data

Comparison of our data with previous work on the mass-dependent Ti isotopic composition of meteorites of Williams (2014) (PhD Thesis, Table 5.1, page 156) is complicated by the fact that different isotopic ratios and standards were used. Thus, the data of Williams (2014) was renormalized to the OL-Ti standard by applying an offset of -0.208 ‰ corresponding to the average difference in δ^{49}Ti values measured in USGS geostandards BHVO-2 and BCR-2 between Williams (2014) and Millet et al. (2016). As error estimate for the Williams (2014) data we use the reported δ^{49}Ti uncertainty of the Ti reference standard (Ti wire), i.e. ± 0.06 ‰. The renormalized data of Williams (2014) give δ^{49}Ti values of carbonaceous chondrites, ordinary chondrites, rumuruti chondrites, basaltic eucrites and an acapulcoite, that range between +0.08

± 0.06 ‰ and -0.03 ± 0.06 ‰. Thus, all meteorites analyzed by Williams (2014) overlap within errors and agree with our results. However, their data shows two populations with respect to δ^{49}Ti values, one with heavier values of around +0.07 ‰ including Allende (CV), Murchison (CM), Allegan (OC, H5) and Dhofar 125 (Acapulcoite) and one with lighter values of around 0.00 ‰ for Richardton (OC, H5), NWA 755 (Rumuruti chondrite), NWA 753 (Rumuruti chondrite), Pasamonte (Eucrite) and Juvinas (Eucrite), which taken at face value would indicate larger heterogeneity in the δ^{49}Ti value of solar system objects than observed in our study. Based on our set of samples, including chondrites, various achondrites and terrestrial komatiites (Fig. 7, Table 4), we argue that solar objects are defined by a homogeneous Ti isotopic composition.

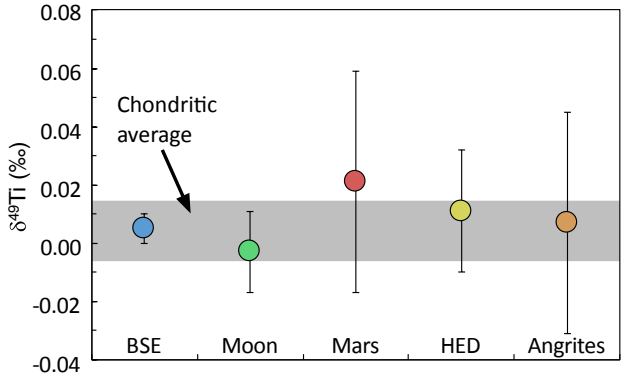

Figure 7: Estimated average Ti isotopic compositions of the angrite and HED parent bodies, Mars, the Moon and the bulk silicate Earth (BSE), compared to the chondritic composition. The lack of variations indicates that given current analytical precision, solar system objects have uniform Ti isotopic compositions. Magmatic fractionation of Ti isotopes in the Aubrite parent-body prevent us from assessing its bulk composition.

6 Conclusion

1. A new sample preparation technique for measuring the stable isotopic composition of titanium is presented. Samples are digested using $LiBO_2$ flux fusion, which leads to complete dissolution of chemically resistant accessory minerals and avoids the creation of insoluble Ti-bearing fluorides that may fractionate Ti isotopes.

2. No difference in the Ti isotopic composition among ordinary, enstatite, and carbonaceous chondrites is observed, except possibly for the CV chondrite Allende, which is rich in CAIs. The average chondritic δ^{49}Ti value of +0.004 ± 0.010 ‰ is identical to that of the HED parent-body (+0.011± 0.021 ‰) the angrite parent-body (+0.007 ± 0.038 ‰), Mars (+0.021 ± 0.038 ‰) and published estimates for the Moon (-0.003 ± 0.014 ‰) and the bulk silicate Earth (+0.005 ± 0.005 ‰). The homogeneous Ti isotopic composition among all classes of chondrites contrasts with published Ca isotope data showing that carbonaceous chondrites are shifted towards lighter Ca isotopic compositions compared to Earth, ordinary, and enstatite chondrites. The decoupling of the Ti and Ca isotope systems likely originated from differences in behaviors between Ca and Ti during condensation in the solar nebula.

3.The Ti isotopic variations observed among aubrite meteorites span about ~0.3 ‰, which is much larger than the range found in terrestrial basalts and HED meteorites. The reason for the more fractionated isotopic compositions is that differentiation and magmatic fractionation on the aubrite parent-body occurred under highly reducing conditions, allowing partially chalcophile Ti^{3+} and lithophile Ti^{4+} to co-exist. The good negative correlation between δ^{49}Ti values and the MgO/SiO_2 ratios and MgO concentrations is interpreted to be due to redox isotope fractionation, whereby magmatic differentiation results in enrichment of isotopically heavy Ti^{4+} in the residual melt.

4. Titanium isotopic fractionation during ilmenite precipitation during late stages of lunar magma ocean crystallization resulted in a progressive enrichment of heavy Ti isotopes in the residual melt, as is evident from the observed heavy δ^{49}Ti value of KREEPy impact melt breccia Sau 169 (+0.330 ± 0.034 ‰).

Acknowledgments

This work was supported by the Swiss National Science Foundation, grant P2BEP2_158983 to NDG; NSF (CSEDI, grant EAR1502591; Petrology and Geochemistry, grant EAR1444951) and NASA (LARS, grant NNX17AE86G, EW NNX17AE87G, and SSW NNX15AJ25G) grants to ND. The Robert A. Pritzker Center for Meteoritics and Polar Studies at the Field Museum and P. Heck, the Muséum National d'Histoire Naturelle and the Smithsonian Institute are thanked for providing meteorite samples. Discussions with M.-A. Millet, Steven Simon and J.A. Barrat were greatly appreciated. We thank Gary Byerly, Carl Anhaeusser, and Euan Nisbet for making samples from the Barberton and Belingwe greenstone belts available for this study. Constructive criticisms by three anonymous

reviewers helped improve the manuscript. Editorial assistance by Stefan Weyer is also appreciated.

References

Arndt, N.T., (1986). Differentiation of komatiite flows. Journal of Petrology, 27(2), 279-301.

Arndt, N.T., Naldrett, A.J., Pyke, D.R., 1977. Komatiitic and iron-rich tholeiitic lavas of Munro Township, northeast Ontario. J. Petrol. 18, 319–369.

Barrat, J. A., Dauphas, N., Gillet, P., Bollinger, C., Etoubleau, J., Bischoff, A., and Yamaguchi, A., 2016. Evidence from Tm anomalies for non-CI refractory lithophile element proportions in terrestrial planets and achondrites. Geochimica et Cosmochimica Acta, 176, 1-17.

Beard, B. L., Taylor, L. A., Scherer, E. E., Johnson, C. M., and Snyder, G. A., 1998. The source region and melting mineralogy of high-titanium and low-titanium lunar basalts deduced from Lu-Hf isotope data. Geochimica et Cosmochimica Acta, 62(3), 525-544.

Berry, A.J., Walker, A.M., Hermann, J., O'Neill, H.S.C., Foran, G.J., Gale, J.D., 2007. Titanium substitution mechanisms in forsterite. Chemical Geology 242, 176–186.

Chianelli, R.R., Scanlon, J.C. and Thompson, A.H., 1975. Structure refinement of stoichiometric TiS2. Materials Research Bulletin, 10, 1379–1382.

Clayton, R. N., Mayeda, T. K., and Rubin, A. E., 1984. Oxygen isotopic compositions of enstatite chondrites and aubrites. In Lunar and Planetary Science Conference Proceedings 15, C245-C249.

Cormier, L., Calas, G., Neuville, D.R., and Bellisent, R., 2001. A high temperature neutron diffraction study of a titanosilicate glass, Journal of Non-Crystalline Solids, 293-295, 510-516.

Consolmagno, G. J., and Drake, M. J., 1977. Composition and evolution of the eucrite parent body: Evidence from rare earth elements. Geochimica et Cosmochimica Acta, 41(9), 1271-1282.

Daswani, M. M., Heck, P. R., Greber, N. D., and Greenwood, R. C., 2017. Petrography and geochemistry of Northwest Africa 11115: A new, enriched, high thorium basaltic shergottite. 80th Annual Meeting of the Meteoritical Society, Santa Fe (USA). Abstract #6302.

Dauphas, N., Chen, J. H., Zhang, J., Papanastassiou, D. A., Davis, A. M., and Travaglio, C., 2014a. Calcium-48 isotopic anomalies in bulk chondrites and achondrites: evidence for a uniform isotopic reservoir in the inner protoplanetary disk. Earth and Planetary Science Letters, 407, 96-108.

Dauphas, N., Roskosz, M., Alp, E.E., Neuville, D.R., Hu, M.Y., Sio, C.K., Tissot, F.L.H., Zhao, J., Tissandier, L., Médard, E., Cordier, C., 2014b. Magma redox and structural controls on iron isotope variations in Earth's mantle and crust. Earth and Planetary Science Letters 398, 127–140.

Dauphas, N., Pourmand, A., and Teng, F., Z., 2009. Routine isotopic analysis of iron by HR-MC-ICPMS: How precise and how accurate?. Chemical Geology, 267(3), 175-184.

Dauphas, N., Pourmand, A., 2015. Thulium anomalies and rare earth element patterns in meteorites and Earth: Nebular fractionation and the nugget effect. Geochimica et Cosmochimica Acta 163, 234–261.

Dauphas, N., and Schauble, E. A., 2016. Mass Fractionation Laws, Mass-Independent Effects, and Isotopic Anomalies. Annual Review of Earth and Planetary Sciences, 44.

Dauphas, N., Teng, F.-Z., and Arndt, N., 2010. Magnesium and iron isotopes in 2.7 Ga Alexo komatiites: Mantle signatures, no evidence for Soret diffusion, and identification of diffusive transport in zoned olivine. Geochimica et Cosmochimica Acta 74.

Davis, A.M., Zhang, J., Hu, J., Greber, N.D., and Dauphas, N., 2016. Titanium Isotopic Anomalies, Titanium Mass Fractionation Effects, and Rare Earth Element Patterns in Allende CAIs and Their Relationships. In: Lunar and Planetary Science XL. Abstract #3032.

Elkins-Tanton, L. T., Burgess, S., and Yin, Q. Z., 2011. The lunar magma ocean: Reconciling the solidification process with lunar petrology and geochronology. Earth and Planetary Science Letters, 304(3), 326-336.

Elkins-Tanton, L.T., Hagger, B.H., and Grove, T.L., 2004. Magmatic effects of the lunar late heavy bombardment, Earth and Planetary Science Letters 222, 17–27.

Farges, F., Brown Jr., G.E., Rehr, J.J., 1996. Coordination chemistry of Ti (IV) in silicate glasses and melts: I. XAFS study of titanium coordination in oxide model compounds. Geochimica et Cosmochimica Acta 60 (16), 3023–3038.

Farges, F., Brown Jr., G.E., 1997. Coordination chemistry of titanium (IV) in silicate glasses and melts: IV. XANES studies of synthetic and natural volcanic glasses and tektites at ambients temperature and pressure. Geochimica et Cosmochimica Acta 61 (9), 1863–1870.

Fourny, A., Weis, D., Scoates, J.S., 2016. Comprehensive Pb-Sr-Nd-Hf isotopic, trace element, and mineralogical characterization of mafic to ultramafic rock reference materials. Geochemistry Geophysics Geosystems 17, 739–773.

Gall, L., Williams, H. M., Halliday, A. N., and Kerr, A., C., 2016. Nickel isotopic composition of the mantle. Geochimica et Cosmochimica Acta.

Gnos, E., Hofmann, B. A., Al-Kathiri, A., Lorenzetti, S., Eugster, O., Whitehouse, M.J., Villa, I.M., Jull, A.J.T., Eikenberg, J., Spettel, B., Krähenbühl, U., Franchi, I.A., Greenwood, G.C., 2004. Pinpointing the source of a lunar meteorite: implications for the evolution of the Moon, Science, 305(5684), 657-659.

Greber, N.D., Puchtel, I.S., Nägler, T.F., Mezger, K., 2015. Komatiites constrain molybdenum isotope composition of the Earth's mantle. Earth and Planetary Science Letters 421, 129–138.

Green, T.H., 1994. Experimental studies of trace-element partitioning applicable to igneous petrogenesis—Sedona 16 years later. Chemical Geology 117, 1-36.

Grossman, L., Larimer, J.W., 1974. Early chemical history of the solar system, Reviews of Geophysics and Space Physics 12(1), 71-99.

Hallis, L.J., Annand, M., and Strekopytov, S., 2014. Trace-element modeling of mare basalt parental melts: implications for a heterogeneous lunar mantle. Geochimica et Cosmochimica Acta 134, 289–316.

Helffrich, G. R., and Wood, B. J., 2001, The Earth's mantle. Nature 421, 501-507

Hermann, J., Gerald, J., Malaspina, N., Berry, A.J., 2007. OH-bearing planar defects in olivine produced by the breakdown of Ti-rich humite minerals from Dabie Shan (China). Contributions to Mineralogy and Petrology 153, 417-428.

Hess, P.C., and Parmentier, E.M., 1995. A model for the thermal and chemical evolution of the Moon's interior: implications for the onset of mare volcanism, Earth and Planetary Science Letters 134, 501–514.

Hezel D.C., Russell S.S., Ross A.J., Kearsley A.T. 2008, Modal abundances of CAIs: Implications for bulk chondrite element abundances and fractionations. Meteoritics and Planetary Science 43, 1879-1894

Huang, S., Farkaš, J., Yu, G., Petaev, M.I., Jacobsen, S.B., 2012. Calcium isotopic ratios and rare earth element abundances in refractory inclusions from the Allende CV3 chondrite. Geochimica et Cosmochimica Acta 77, 252–265.

Huang, S., Jacobsen, S.B., 2017. Calcium isotopic compositions of chondrites. Geochimica et Cosmochimica Acta 201, 364–376.

Jarosewich, E., Clarke Jr., R.S., Barrows, J.N., 1987. The Allende meteorite reference sample. Smithsonian Contributions to Earth Sciences, 27, 1–49

Kato, C., Moynier, F., Foriel, J., Teng, F. Z., and Puchtel, I., S., 2016. The gallium isotopic composition of the bulk silicate Earth. Chemical Geology.

Keil, K., 1989. Enstatite meteorites and their parent bodies. Meteoritics 24, 195-208.

Keil, K., 2010. Enstatite achondrite meteorites (aubrites) and the histories of their asteroidal parent bodies. Chemie der Erde - Geochemistry 70, 295–317.

Keil, K., 2012. Angrites, a small but diverse suite of ancient, silica-undersaturated volcanic-plutonic mafic meteorites, and the history of their parent asteroid. Chemie der Erde, 72(3), 191-218.

Korotev, R., L., 2005. Lunar geochemistry as told by lunar meteorites. Chemie der Erde-Geochemistry, 65(4), 297-346.

Kuehner, S. M., and Irving, A. J., 2007. Grain Boundary Glasses in the Plutonic Angrite NWA 4590: Evidence for Rapid Decompressive Partial Melting and Cooling on Mercury?. In Lunar and Planetary Science Conference (Vol. 38, p. 1522).

Lahaye, Y., Arndt, N., 1996. Alteration of a komatiite flow from Alexo, Ontario, Canada. Journal of Petrology 57(6), 1261-1284.

Leya, I., Schönbächler, M., Wiechert, U., Krähenbühl, U., and Halliday, A. N., 2008. Titanium isotopes and the radial heterogeneity of the solar system. Earth and Planetary Science Letters, 266(3), 233-244.

Lin, Y., Shen, W., Liu, Y., Xu, L., Hofmann, B. A., Mao, Q., Tang, G. Q., Wu, F., and Li, X. H., 2012. Very High-K KREEP-Rich Clasts in the Impact Melt Breccia of the Lunar Meteorite SaU 169: New Constraints on the Last Residue of the Lunar Magma Ocean. Geochimica et Cosmochimica Acta 85, 19-40.

Lodders, K., Palme, H., and Wlotzka, F., 1993. Trace elements in mineral separates of the Pena Blanca Spring aubrite: Implications for the evolution of the aubrite parent body. Meteoritics, 28(4), 538-551.

Lodders, K., 2003. Solar system abundances and condensation temperatures of the elements. The Astrophysical Journal 591, 1220-1247

Lugmair, G. W., and Shukolyukov, A., 1998. Early solar system timescales according to ^{53}Mn-^{53}Cr systematics. Geochimica et Cosmochimica Acta, 62(16), 2863-2886.

Mandler, B.E., Elkins-Tanton, L.T., 2013. The origin of eucrites, diogenites, and olivine diogenites: Magma ocean crystallization and shallow magma chamber processes on Vesta. Meteoritics & Planetary Science 48, 2333–2349.

McDonough, W. F., and Sun, S., S., 1995. The composition of the Earth. Chemical geology, 120(3), 223-253.

McDonough, W.F., Stosch, H.G., Ware, N.G., 1992. Distribution of titanium and the rare earth elements between peridotitic minerals. Contributions to Mineralogy and Petrology 110, 321-328

Millet, M.-A., Doucelance, R., Schiano, P., David, K., Bosq, C., 2008. Mantle plume heterogeneity versus shallow-level interactions: a case study, the São Nicolau Island, Cape Verde archipelago. Journal of Volcanology and Geothermal Research 176 (2), 265–276.

Millet, M.-A., Doucelance, R., Baker, J.A., Schiano, P., 2009. Reconsidering the origins of isotopic variations in Ocean Island Basalts: insights from fine-scale study of São Jorge Island, Azores archipelago. Chemical Geology 265 (3–4), 289–302.

Millet, M.-A., Dauphas, N., 2014. Ultra-precise titanium stable isotope measurements by double-spike high resolution MC-ICP-MS. Journal of Analytical Atomic Spectrometry 29, 1444.

Millet, M.-A., Dauphas, N., Greber, N.D., Burton, K.W., Dale, C.W., Debret, B., Macpherson, C.G., Nowell, G.M., Williams, H.M., 2016. Titanium stable isotope investigation of magmatic processes on the Earth and Moon. Earth and Planetary Science Letters 449, 197–205.

Mittlefehldt, D.W., 2005. Ibitira: A basaltic achondrite from a distinct parent asteroid and implications for the Dawn mission. Meteoritic & Planetary Science 40, 665– 677.

Mittlefehldt, D.W., 2015. Asteroid (4) Vesta: I. The howardite-eucrite-diogenite (HED) clan of meteorites. Chemie der Erde - Geochemistry 75, 155–183.

Niederer, F. R., and Papanastassiou, D. A., 1984. Ca isotopes in refractory inclusions. Geochimica et Cosmochimica Acta, 48(6), 1279-1293.

Niederer, F. R., Papanastassiou, D. A., and Wasserburg, G. J., 1985. Absolute isotopic abundances of Ti in meteorites. Geochimica et Cosmochimica Acta, 49(3), 835-851.

Okada, A., Keil, K., Taylor, G.J., Newsom, H., 1988. Igneous history of the aubrite parent asteroid: Evidence from the Norton County enstatite achondrite. Meteoritics 23, 59-74.

O'Neill, H.St.C., Navrotsky, A., 1983. Simple spinels — crystallographic parameters, cation radii, lattice energies, and cation distribution. American Mineralogist 68, 181–194.

Papike, J.J., Simon, S.B., Burger, P.V., Bell, A.S., Shearer, C.K., Karner, J.M., 2016. Chromium, vanadium, and titanium valence systematics in Solar System pyroxene as a recorder of oxygen fugacity, planetary provenance, and processes. American Mineralogist 101, 907–918

Pourmand, A., Dauphas, N., and Ireland, T., J., 2012. A novel extraction chromatography and MC-ICP-MS technique for rapid analysis of REE, Sc and Y: Revising CI-chondrite and Post-Archean Australian Shale (PAAS) abundances. Chemical Geology, 291, 38-54.

Puchtel, I.S., Blichert-Toft, J., Touboul, M., Walker, R.J., Byerly, G.R., Nisbet, E.G., Anhaeusser, C.R., 2013. Insights into early Earth from Barberton komatiites: Evidence from lithophile isotope and trace element systematics. Geochimica et Cosmochimica Acta 108, 63–90.

Puchtel, I.S., Walker, R.J., Touboul, M., Nisbet, E.G., Byerly, G.R., 2014. Insights into early Earth from the Pt-Re-Os isotope and highly siderophile element abundance systematics of Barberton komatiites. Geochimica et Cosmochimica Acta 125, 394–413.

Puchtel, I.S., Blichert-Toft, J., Touboul, M., Horan, M.F., Walker, R.J., 2016. The coupled 182W-142Nd record of early terrestrial mantle differentiation. Geochemistry Geophysics Geosystems, 1–26.

Puchtel, I.S., Walker, R.J., Brandon, A.D., and Nisbet, E.G., 2009. Pt–Re–Os and Sm–Nd isotope and HSE and REE systematics of the 2.7 Ga Belingwe and Abitibi komatiites, Geochimica et Cosmochimica Acta, 73(20), 6367-6389.

Raczek, I., Stoll, B., Hofmann, A.W., Peter Jochum, K., 2007. High-Precision Trace Element Data for the USGS Reference Materials BCR-1, BCR-2, BHVO-1, BHVO-2, AGV-1, AGV-2, DTS-1, DTS-2, GSP-1 and GSP-2 by ID-TIMS and MIC-SSMS. Geostandards and Geoanalytical Research 25, 77–86.

Richter, F.M., Dauphas, N., Teng, F.-Z., 2009. Non-traditional fractionation of non-traditional isotopes: Evaporation, chemical diffusion and Soret diffusion. Chemical Geology 258, 92–103.

Robin-Popieul, C.C.M., Arndt, N., Chauvel, C., Byerly, G.R., Sobolev, A.V., Wilson, A., 2012. A New Model for Barberton Komatiites: Deep Critical Melting with High Melt Retention. Journal of Petrology 53, 2191–2229.

Rudnick, R. L., and Gao, S., 2003. Composition of the Continental Crust. Treatise on Geochemistry, 3, 659.

Schauble, E.A., 2004. Applying stable isotope fractionation theory to new systems. Reviews in Mineralogy and Geochemistry 55, 65-111.

Shearer, C. K., and Papike, J. J., 1999. Magmatic evolution of the Moon, American Mineralogist, 84(10), 1469-1494.

Shirai, N., Humayun, M., and Irving, A. J., 2009. The bulk composition of coarse-grained meteorites from laser ablation analysis of their fusion crusts. In Lunar and Planetary Science Conference (Vol. 40, p. 2170).

Simon, J.I., Jordan, M. K., Tappa, M. J., Kohl, I. E., and Young, E. D. 2016a. Calcium and Titanium Isotope Fractionation in CAIS: Tracers of Condensation and Inheritance in the Early Solar Protoplanetary Disk. In: Lunar and Planetary Science XL. Abstract #1397.

Simon, J.I., DePaolo, D.J., 2010. Stable calcium isotopic composition of meteorites and rocky planets. Earth and Planetary Science Letters 289, 457–466.

Simon, S.B., Grossman, L., and Davis, A.M., 1991 Fassaite composition trends during crystallization of Allende Type B refractory inclusion melts. Geochimica et Cosmochimica Acta, 55, 2635–2655.

Simon, S.B., Sutton, S.R., Grossman, L., 2016b. The valence and coordination of titanium in ordinary and enstatite chondrites. Geochimica et Cosmochimica Acta 189, 377–390.

Snyder, G.A., Taylor, L.A., Neal, C.R., 1992. A chemical model for generating the sources of mare basalts: combined equilibrium and fractional crystallization of the lunar magmasphere, Geochimica et Cosmochimica Acta 56, 3809–3823.

Takahashi, T., and Yamada, O., 1973. Crystallographic and magnetic properties of the Cd(OH)2 layer structure compound TiS_2 containing extra iron, Journal of Solid State Chemistry, 7, (1973) 25-30.

Tang, H., and Dauphas, N., 2012. Abundance, distribution, and origin of ^{60}Fe in the solar protoplanetary disk. Earth and Planetary Science Letters, 359, 248-263.

Tarantino, S. C., Domeneghetti, M. C., Carpenter, M. A., Shaw, C. J., and Tazzoli, V., 2002. Mixing properties of the enstatite-ferrosilite solid solution: I. A macroscopic perspective. European Journal of Mineralogy, 14(3), 525-536.

Teng, F-Z., Dauphas N., and Watkins J.M., 2017. Non-Traditional Stable Isotopes: Retrospective and Prospective. Reviews in Mineralogy and Geochemistry, 82.1, 1-26.

Tissot, F. L., and Dauphas, N., 2015. Uranium isotopic compositions of the crust and ocean: Age corrections, U budget and global extent of modern anoxia. Geochimica et Cosmochimica Acta, 167, 113-143.

Trinquier, A., Elliott, T., Ulfbeck, D., Coath, C., Krot, A. N., and Bizzarro, M., 2009. Origin of nucleosynthetic isotope heterogeneity in the solar protoplanetary disk. Science, 324(5925), 374-376.

Trinquier, A., Birck, J. L., Allègre, C. J., Göpel, C., and Ulfbeck, D., 2008. ^{53}Mn–^{53}Cr systematics of the early Solar System revisited. Geochimica et Cosmochimica Acta, 72(20), 5146-5163.

Trinquier, A., Birck, J. L., & Allègre, C., J., 2007. Widespread ^{54}Cr heterogeneity in the inner solar system. The Astrophysical Journal, 655(2), 1179.

Turner, S., Hawkesworth, C., Rogers, N., King, P., 1997. U–Th isotope disequilibria and ocean island basalt generation in the Azores. Chemical Geology 139 (1–4), 145–164.

Valdes, M.C., Moreira, M., Foriel, J., Moynier, F., 2014. The nature of Earth's building blocks as revealed by calcium isotopes. Earth and Planetary Science Letters 394, 135–145.

Van Orman, J.A., and Grove, T.L., 2000. Origin of lunar high-titanium ultramafic glasses: constraints from phase relations and dissolution kinetics of clinopyroxene-ilmenite cumulates, Meteoritic and Planetary Sciences, 35, 783–794.

Wagner, T.P., and Grove, T.L., 1997. Experimental constraints on the origin of lunar high-Ti ultramafic glasses, Geochimica et Cosmochimica Acta 61, 1315–1327.

Warren, P. H., and Wasson, J. T., 1979. The origin of KREEP, Reviews of Geophysics, 17(1), 73-88.

Wasson, J. T., and Kallemeyn, G., W., 1988. Compositions of chondrites. Philosophical Transactions of the Royal Society of London A: Mathematical, Physical and Engineering Sciences, 325(1587), 535-544.

Watters, T. R., and Prinz, M., 1979. Aubrites-Their origin and relationship to enstatite chondrites. In Lunar and Planetary Science Conference Proceedings, 10, 1073-1093.

Waychunas, G.A., 1987. Synchrotron radiation XANES spectroscopy of Ti in minerals: effects of Ti bonding distances, Ti valence, and site geometry on absorption edge structure. American Mineralogist 72, 89–101.

Weyer, S., and Ionov, D., A., 2007. Partial melting and melt percolation in the mantle: the message from Fe isotopes. Earth and Planetary Science Letters, 259(1), 119-133.

Wiechert, U. H., Halliday, A. N., Palme, H., and Rumble, D., 2004. Oxygen isotope evidence for rapid mixing of the HED meteorite parent body. Earth and Planetary Science Letters, 221(1), 373-382.

Williams, N.H., 2014. Titanium Isotope Cosmochemistry, PhD Dissertation, School of Earth, Atmospheric and Environmental Sciences, The University of Manchester, England

Winter, J. D. 2001. *An introduction to igneous and metamorphic petrology*. Upper Saddle River, NJ: Prentice Hall.

Young, E. D., Manning, C. E., Schauble, E. A., Shahar, A., Macris, C. A., Lazar, C., and Jordan, M., 2015. High-temperature equilibrium isotope fractionation of non-traditional stable isotopes: Experiments, theory, and applications. Chemical Geology, 395, 176-195.

Zhang, J., Dauphas, N., Davis, A.M., Pourmand, A., 2011. A new method for MC-ICPMS measurement of titanium isotopic composition: Identification of correlated isotope anomalies in meteorites, Journal of Analytical Atomic Spectrometry 26, 2197.

Zhang J. 2012. Titanium isotope cosmochemistry. PhD Dissertation, Department of Geophysical Sciences, University of Chicago, USA

Zhang, J., Dauphas, N., Davis, A.M., Leya, I., Fedkin, A., 2012. The proto-Earth as a significant source of lunar material, Nature Geoscience 5, 251–255.

Tables

Table 1: Titanium isotopic compositions of chondrites

Sample	Group	ε^{46}Ti	95% c.i.	ε^{48}Ti	95% c.i.	δ^{49}Ti^{a} (‰)	δ^{49}Ti (‰)	95% c.i.	n
Ste Marguerite	H4	-0.08	0.01	-0.02	0.12	0.029	0.022	0.033	4
Queen's Mercy	H6	-0.08	0.01	-0.02	0.12	0.002	-0.005	0.033	4
Pultusk	H5	-0.08	0.01	-0.02	0.12	-0.008	-0.015	0.033	4
Bald Mountain	L4	-0.08	0.01	-0.02	0.12	-0.020	-0.027	0.033	4
Farmington	L5	-0.08	0.01	-0.02	0.12	0.012	0.005	0.033	4
Kelly	LL4	-0.08	0.01	-0.02	0.12	0.014	0.007	0.033	4
Dhurmsala	LL6	-0.08	0.01	-0.02	0.12	0.021	0.014	0.033	4
Chelyabinsk	LL5	-0.08	0.01	-0.02	0.12	0.018	0.011	0.033	4
Chelyabinsk*	LL5	-0.08	0.01	-0.02	0.12	0.022	0.015	0.037	4
Sahara 97072	EH3	0.01	0.02	-0.02	0.06	0.023	0.026	0.034	4
Blithfield	EL6	0.01	0.02	-0.02	0.06	0.024	0.027	0.034	4
Pillistfer	EL6	0.01	0.02	-0.02	0.06	-0.022	-0.019	0.034	4
Lancé	CO	0.61	0.05	-0.07	0.16	-0.075	0.002	0.036	4
Murray	CM	0.56	0.05	-0.08	0.16	-0.075	-0.002	0.036	4
Orgueil	CI	0.35	0.04	0.00	0.15	-0.032	0.009	0.034	4
Allende	CV	0.72	0.02	0.02	0.08	-0.028	0.052	0.032	4
Average							*0.007*	*0.011*	
Average (excluding Allende)							*0.004*	*0.010*	

δ^{49}Ti^{a}: Ti isotopic composition prior to correction for isotopic anomalies on ^{46}Ti and ^{48}Ti.

ε^{46}Ti and ε^{48}Ti isotope anomalies from Zhang et al., (2012)

95% c.i.= 95% confidence interval

*Sample spiked prior to flux fusion

n is the number of repeat measurements of the purified Ti solution.

Table 2: Titanium isotopic composition of komatiite samples and selected USGS rock reference standards

Sample	Location	Facies	δ^{49}Ti (‰)	95% c.i.	n
SCH1.1	Schapenburg	Sp	0.005	0.030	4
SCH1.5		Sp	0.029	0.030	4
SCH1.6		Sp	0.032	0.030	4
SCH2.1		Sp	0.001	0.030	8
SCH2.2		Sp	0.036	0.030	4
SCH2.3		Sp	0.050	0.030	4
Average Schapenburg			*0.025*	*0.020*	
BV03	Komati	OC	0.009	0.030	8
BV04A		Sp	-0.001	0.030	4
BV04B		Sp	0.008	0.030	4
BV05		Sp	0.022	0.030	4
BV06		CM	-0.029	0.030	4
Average Komati			*0.002*	*0.024*	
564-6	Weltevreden	CM	-0.015	0.034	4
501-1*		OC	-0.072	0.030	4
501-1[b]			0.004	0.033	4
501-2		OC	-0.022	0.030	4
501-3		Sp	-0.039	0.030	4
501-4		Sp	-0.017	0.030	4
501-8*		OC	-0.102	0.030	4
501-8[b]			-0.001	0.033	4
Average Weltevreden			*-0.015*	*0.012*	
TN01	Belingwe	CM	0.030	*0.034*	4
TN03		Sp	0.009	*0.034*	4
TN21		OC	0.017	*0.034*	4
ZV10		OC	0.005	*0.034*	4
ZV14		Sp	0.017	*0.034*	4
Average Belingwe			*0.016*	*0.012*	
M657	Alexo	Sp	-0.034	0.030	4
M657[b]			-0.011	0.033	4
M663		Sp	-0.074	0.030	4
M663[b]			-0.030	0.033	4
M666		CM	-0.060	0.030	4
M666[b]			-0.040	0.033	4
M712		OC	-0.035	0.030	4
M712[b]			0.000	0.033	4
Average Alexo			*-0.035*	*0.015*	
BHVO-2	USGS		0.015	0.025	44
BIR-1a	USGS		-0.065	0.025	40
G3	USGS		0.429	0.025	25

Sp: spinifex textured rock, OC: olivine cumulate, CM: chilled margin

95% c.i.= 95% confidence interval

USGS: USGS powder rock reference standards, agree well with those published in Millet et al., (2014) and Millet et al., (2016)

*samples exclude for calculation of average value

b: duplicate measurement, prepared from new pellet aliquot

n is the number of repeat measurements of the purified Ti solution.

Table 3: Titanium isotopic compositions of lunar and achondrite samples

Sample	Classification	ε^{46}Ti	95% c.i.	ε^{48}Ti	95% c.i.	δ^{49}Ti[a] (‰)	δ^{49}Ti (‰)	95% c.i.	n
Moon									
SaU 169	KREEP	-	-	-	-	-	0.330	0.034	4
Mars									
NWA11115	Shergottite	-0.17	0.04	-0.07	0.07	0.029	0.021	0.038	4
Angrites									
NWA2999	Plutonic	-0.21	0.04	0.06	0.20	0.017	0.000	0.042	4
NWA4590	Plutonic	-0.21	0.04	0.06	0.20	-0.062	-0.111	0.042	4
D'Orbigny	Volcanic	-0.21	0.04	0.06	0.20	0.081	0.042	0.042	4
Sahara99555	Volcanic	-0.21	0.04	0.06	0.20	0.034	-0.005	0.042	4
NWA1670	Volcanic	-0.21	0.04	0.06	0.20	0.033	-0.010	0.042	4
Average Angrites (NWA4590 excluded)							*0.007*	*0.038*	
HED-meteorites									
Johnstown	Diogenite	-0.22	0.03	-0.05	0.06	0.038	0.019	0.031	4
Tatahouine	Diogenite	-0.22	0.03	-0.05	0.06	0.017	-0.002	0.030	4
Serra de Magé	CM Eucrite	-0.22	0.03	-0.05	0.06	0.042	0.023	0.031	4
Nagaria	CM Eucrite	-0.22	0.03	-0.05	0.06	0.054	0.034	0.031	4
Kapoeta	Howardite	-0.22	0.03	-0.05	0.06	0.063	0.044	0.030	4
Millbillillie	MG Eucrite	-0.22	0.03	-0.05	0.06	0.016	-0.003	0.030	4
Camel Donga	MG Eucrite	-0.22	0.03	-0.05	0.06	0.044	0.025	0.030	4
Juvinas	MG Eucrite	-0.22	0.03	-0.05	0.06	-0.006	-0.025	0.030	4
Lakangaon	NL Eucrite	-0.22	0.03	-0.05	0.06	0.073	0.054	0.031	4
Lakangaon[b]						0.045	0.026	0.033	4
Stannern	ST Eucrite	-0.22	0.03	-0.05	0.06	0.021	0.002	0.031	4
Ibitira		-0.22	0.03	-0.05	0.06	-0.032	-0.051	0.030	4
Ibitira[b]						-0.004	-0.023	0.033	4
Average HED							*0.011*	*0.015*	
Aubrites									
Cumberland Falls		0.01	0.03	-0.05	0.16	0.039	0.046	0.034	4
Bishopville		0.01	0.03	-0.05	0.16	0.235	0.242	0.034	4
Norton County		0.01	0.03	-0.05	0.16	-0.076	-0.069	0.034	4
Peña Blanca Spring		0.01	0.03	-0.05	0.16	0.089	0.096	0.034	4
Bustee		0.01	0.03	-0.05	0.16	0.042	0.049	0.035	4
Shallowater[c]		0.01	0.03	-0.05	0.16	0.058	0.065	0.034	4

δ^{49}Ti[a]: Ti isotopic composition prior to correction for isotopic anomalies on ^{46}Ti and ^{48}Ti

ε^{46}Ti and ε^{48}Ti, isotopic anomalies from Zhang et al., (2012) except Mars, which is from Trinquier et al., (2009)

b: Duplicate measurement, prepared from new pellet aliquot

c: Shallowater may originate from a distinct parent-body than rest of group, see text for explanation

95% c.i.= 95% confidence interval

CM = cumulate; MG = main group; NL = Nuevo Laredo group; ST = Stannern group

n is the number of repeat measurements of the purified Ti solution.

Table 4: Estimated average Ti isotopic compositions for komatiites, chondrites, the Moon, Mars and parent bodies of HED and angrite meteorites

	δ^{49}Ti (‰)	95% c.i.
Komatiites	-0.001	0.019
Chondrites	0.004	0.010
Moon*	-0.003	0.014
Mars	0.021	0.038
HED	0.011	0.015
Angrite	0.007	0.038
Average	*0.007*	*0.007*
*Bulk silicate Earth**	*0.005*	*0.005*

*Data from Millet et al. (2016)

Appendix

Appendix A. Double-spike correction in the presence of isotopic anomalies.

Let us write $R^{i/47}_{Standard}$ and $R^{i/47}_{Sample}$ the $^{i}Ti/^{47}Ti$ ratios in the standard and sample. The manner in which isotopic anomalies are calculated is usually by internal normalization, which consists in arbitrarily correcting one ratio for apparent mass fractionation and applying the same mass fractionation correction to all isotope ratios. For a sample, the internally normalized corrected value $R^{i/47\,*}_{Sample}$ would be $R^{i/47\,*}_{Sample} = R^{i/47}_{Sample}/(m^{i}/m^{47})^{\alpha}$, where α is calculated independently by fixing the $^{49}Ti/^{47}Ti$ ratio of the sample to the standard ratio by applying the same formula. Isotopic anomalies are usually expressed as,

$$\varepsilon^{i/47}_{Sample} = \left(\frac{R^{i/47*}_{Sample}}{R^{i/47}_{Standard}} - 1\right) \cdot 10^{4} \cong 10^{4} \ln\left(\frac{R^{i/47*}_{Sample}}{R^{i/47}_{Standard}}\right).$$

We therefore can write $R^{i/47}_{Sample}$ as,

$$R^{i/47}_{Sample} = R^{i/47}_{Standard} \cdot \left(\frac{m_i}{m_{47}}\right)^{\alpha} \cdot \left(1 + \frac{\varepsilon^{i/47}_{Sample}}{10^{4}}\right) \cong R^{i/47}_{Standard} \cdot \left(\frac{m_i}{m_{47}}\right)^{\alpha} \cdot e^{\varepsilon^{i/47}_{Sample}/10^{4}}.$$

This formula is used in double spike data reduction to calculate $R^{i/47}_{Sample}$.

Appendix B. Tables

Table B.1: Ti isotopic compositions of samples prepared by acid attack dissolution and flux fusion, USGS rock reference standards, NIST SRM 3162a and matrix tests (see text for further explanation)

Sample	δ^{49}Ti (‰)	95% c.i.	n
NIST SRM 3162a	1.056	0.026	12
BHVO acid	0.017	0.029	4
BHVO Flux	0.015	0.025	44
BHVO Flux cut1	-0.001	0.029	2
BHVO Flux cut2	0.003	0.029	2
BHVO Flux cut3	0.009	0.029	2
BIR-1a acid	-0.054	0.029	4
BIR-1a Flux	-0.065	0.025	40
BIR-1a Flux cut1	-0.103	0.029	2
BIR-1a Flux cut2	-0.092	0.029	2
BIR-1a Flux cut3	-0.070	0.029	2
G3 Flux	0.429	0.025	25
G3 Flux cut1	0.412	0.029	2
G3 Flux cut2	0.419	0.029	2
G3 Flux cut3	0.431	0.029	2
Flux Blank doped	0.008	0.029	4
M712 Matrix doped	0.009	0.029	4
BV05 Matrix doped	0.009	0.029	4
501-2 Matrix doped	-0.001	0.029	4
M712 acid	-0.029	0.030	4
M712 Flux	-0.022	0.030	8
SCH2.1 acid	0.007	0.030	4
SCH2.1 Flux	-0.006	0.030	4
BV03 acid	0.022	0.030	4
BV03 Flux	-0.005	0.030	4
501-2 acid	-0.016	0.030	4
501-2 Flux	-0.029	0.030	4

95% c.i.= 95% confidence interval

Acid: the sample was digested using acid attack

Flux: the sample was digested using flux fusion

cut1, cut2, cut3: Aliquot of sample was measured after first, second or third ion-exchange chromatography.

n is the number of repeat measurements of the purified Ti solution.

Table B.2: Ti isotopic composition of Ca doping tests, where the Ti standard was doped with different amounts of Ca.

Sample	**^{44}Ca/^{48}Ti**	**% Ca**	**δ^{49}Ti (‰)**	**δ^{49}Ti corr (‰)**	**95% c.i.**
Ca3%	0.00071	3	0.068	0.009	0.029
Ca4%	0.00107	4	0.105	0.011	0.029
Ca5%	0.00155	5	0.154	0.009	0.029
Ca7%	0.00210	7	0.201	0.012	0.029
Ca10%	0.00290	10	0.297	0.028	0.029
Ca20%	0.00571	20	0.585	0.031	0.029
Ca21%	0.00589	21	0.602	0.034	0.029

δ^{49}Ti corr: Ti isotopic composition after correction for Ca interference on ^{46}Ti and ^{48}Ti applying the method described in the manuscript.

%Ca: Mass percent Ca relative to Ti.

Appendix C: Figures

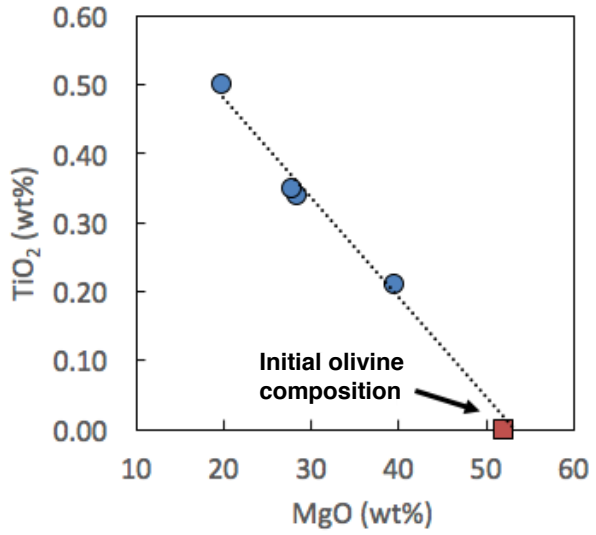

Figure C.1: TiO_2 versus MgO concentrations of analyzed Alexo komatiites (blue circles) and the earliest crystallized olivine (red square). Data from Arndt 1986.

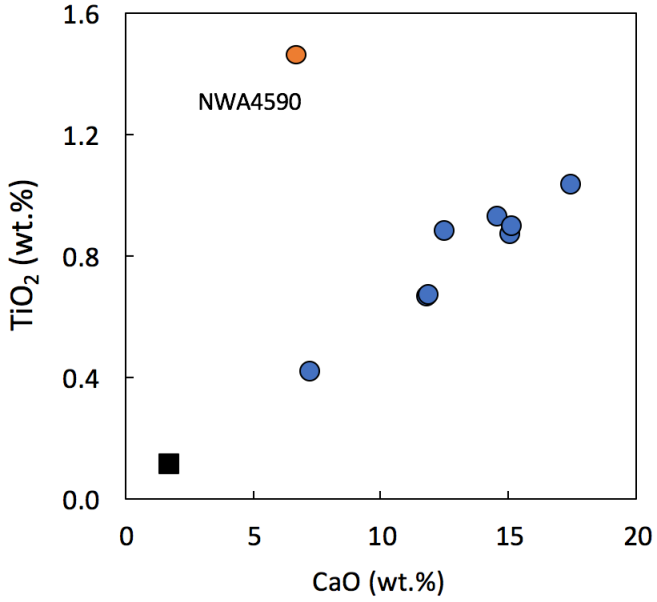

Figure C.2: TiO_2 versus CaO concentrations of angrites (circles; Angra dos Reis not shown). NWA 4590 plots outside the trend of other angrites. The black square is the CI chondrite composition (Wasson and Kallemeyn 1988). Angrite data from Keil (2012).